

# Jets and threshold summation in Deductor

Zoltán Nagy

*DESY, Notkestrasse 85, 22607 Hamburg, Germany* \*

and Davison E. Soper

*Institute of Theoretical Science, University of Oregon, Eugene, OR 97403-5203, USA* †

## Abstract

We explore jet physics in hadron collisions using the parton shower event generator DEDUCTOR. Of particular interest is the one jet inclusive cross section  $d\sigma/dp_T$  for jets of very high  $p_T$ . Compared to the Born level, the cross section decreases substantially because of  $p_T$  loss from the jet during showering. We compare to the same effect in PYTHIA and DIRE. The cross section then increases substantially because of the summation of threshold logarithms included in DEDUCTOR.

We also study the cross section to have a gap with no jets between two hard jets that are widely separated in rapidity. Here we compare DEDUCTOR with virtuality based ordering with DEDUCTOR with  $k_T$  ordering and we check whether adding an underlying event and hadronization has a significant effect beyond that found with just a parton shower.

---

\* [Zoltan.Nagy@desy.de](mailto:Zoltan.Nagy@desy.de)

† [soper@uoregon.edu](mailto:soper@uoregon.edu)

## I. INTRODUCTION

Parton shower Monte Carlo event generators, such as HERWIG [1], PYTHIA [2], and SHERPA [3], perform calculations of cross sections according to an approximation to the standard model or its possible extensions. In most such programs, the shower develops with decreasing values of a parameter that measures of the hardness of interactions: smaller hardness corresponds to a larger scale of space-time separations. Thus a parton shower is essentially an application of the renormalization group. It describes how the description of physics changes as one changes the resolution scale at which a scattering event is examined.

Following this view, we have recently presented a general formulation [4] of how a parton shower can be defined at any order of QCD perturbation theory by using an evolution equation based on operators that characterize the infrared singular behavior of QCD with a variable resolution scale. The current version<sup>1</sup> of the parton shower program DEDUCTOR [5–13] approximately follows this framework, although in its current version its splitting functions are available only to order  $\alpha_s$ .

In DEDUCTOR and other parton shower programs, a hard interaction, based on a new physics model or on the electroweak part of the standard model or on just QCD, initiates an event. At this stage, there are just a few partons. Then, as the hardness decreases, the partons that carry QCD color split, making more partons in a parton shower. Thus the program describes the development of QCD jets.

In this paper, we use DEDUCTOR to explore the description of QCD jets created in a  $2 \rightarrow 2$  QCD hard scattering. We study two problems.

First, we look at the inclusive cross section to produce a jet with a large transverse momentum,  $P_T > 0.3$  TeV with  $\sqrt{s} = 13$  TeV. Here the cross section is falling quickly as  $P_T$  increases because the relevant parton distribution functions are falling quickly. This creates two important effects. One effect is related to the jet definition: any momentum lost from the jet or gained by the jet changes the cross section dramatically. The other effect arises from threshold logarithms, which, in a parton shower, arise from the relation between initial state radiation and the evolution of the parton distribution functions.

Second, we examine the gap survival probability: when two jets are produced with a wide separation  $\Delta y$  in rapidity, this is the probability that there are no other jets between these two with transverse momenta greater than some specified value  $p_T^{\text{cut}}$ . This problem is of interest because

---

<sup>1</sup> Version 2.1.0 of the code, used in this paper, is available at <http://www.desy.de/~znagy/deductor/> and <http://pages.uoregon.edu/soper/deductor/>. Matching to a next-to-leading order perturbative calculation of the hard scattering cross section is included in Ref. [4] but not in DEDUCTOR v. 2.1.0.

its theoretical description involves the summation of logarithms of the ratio of the jet  $P_T$  to  $p_T^{\text{cut}}$  and the summation of the large logarithmic factor  $\Delta y$ . It is not initially evident whether a parton shower approach can provide a good description of this physics. We compare DEDUCTOR results to NLO perturbation theory and to data from Atlas for  $\sqrt{s} = 7$  TeV.

For these studies, we make use of some features of the current version of DEDUCTOR, version 2.1.0, that were not available in earlier versions. First, we can add a simple model for a nonperturbative underlying event and we can include the string model of hadronization provided by PYTHIA. Second, we can compare results obtained with the default hardness measure of DEDUCTOR, which is based on the virtuality in parton splittings, with results obtained with a transverse momentum hardness measure. Here we change only the hardness measure that orders splittings, leaving everything else unchanged. Finally, we include factors that sum threshold logarithms [14–59], which are important when the scale of the hard interaction is large. We included a summation of threshold logs in an earlier paper [13]. In that paper, the infrared behavior of the threshold contributions was not sufficiently well controlled, requiring an infrared cutoff. In this paper, we use an improved version based on the general formulation of Ref. [4]. Then no infrared cutoff is needed. We provide details of the threshold factor in Appendix II C.

## II. NEW FEATURES IN DEDUCTOR

Our analysis is based on the parton shower event generator, DEDUCTOR. In this section, we describe new features of DEDUCTOR that are not described in our previous papers [5–13].

### A. Non-perturbative effects

DEDUCTOR works at the level of perturbative QCD, with perturbative splittings of quarks and gluons. As the splitting scale becomes softer and softer, perturbation theory ceases to be reliable. For this reason, the shower stops when the splittings become too soft: splittings with transverse momenta  $k_T$  smaller than  $k_T^{\text{min}} \approx 1$  GeV are not allowed. If we use the parton shower to make predictions for an infrared safe observable with a large scale, then soft splittings do not matter for this observable and there is little sensitivity to the infrared cutoff. However, the scale associated with an infrared safe observable can sometimes be rather small. Then there can be more sensitivity to physics at the infrared cutoff. To check for this, it may be useful to include non-perturbative effects that represent the effects of physics with scales smaller than  $k_T^{\text{min}}$ .

To check for sensitivity to infrared effects, we need two things. First, we need a model for soft scatterings of partons not involved in the primary hard scattering, the “underlying event.” Second, we need a model for how partons turn into hadrons.

We can include a simple model of an underlying event by using a nonperturbative model designed for this purpose. The model produces a quark and a diquark with large positive rapidity, a quark and a diquark with large negative rapidity, and several gluons with intermediate rapidities. All of these partons carry rather small transverse momenta. This model is, evidently, much less sophisticated than the model in PYTHIA. Code for this underlying event model is included in the DEDUCTOR 2.1.0 distribution as part of the suggested user routines that analyze DEDUCTOR events. Thus a user can easily adjust it.

For hadronization, one can hardly do better than to rely on the color string model in PYTHIA. The color string model is based on a classical color string state  $\{c_f\}_N$  that specifies the color connections among the  $N$  final state partons plus two initial state partons that exist at the end of the shower. What DEDUCTOR gives us is a color density operator basis element  $|\{c\}_N\rangle\langle\{c'\}_N|$  [5–13]. The total probability associated with this color density operator basis element is the corresponding trace of the color density operator,  $\langle\{c'\}_N|\{c\}_N\rangle$ . If we use the leading color approximation, then  $\{c\}_N = \{c'\}_N$ . Given the way that the quantum color states are defined [8], it is then evident that the corresponding classical string state should be  $\{c_f\}_N = \{c\}_N$  to leading power in  $1/N_c^2$ . If we use the LC+ approximation, available in DEDUCTOR, then we can have  $\{c\}_N \neq \{c'\}_N$ . In this case the corresponding total probability  $\langle\{c'\}_N|\{c\}_N\rangle$  is proportional to  $1/N_c^I$  with  $I \geq 1$ . Then our hadronization model can be to use PYTHIA hadronization with  $\{c_f\}_N = \{c\}_N$  with probability 1/2 and with  $\{c_f\}_N = \{c'\}_N$  with probability 1/2. This is in fact the lowest order version of a more general algorithm that is specified in Sec. 8 of Ref. [8]. One could improve this by using a higher order version of this algorithm, but for this paper we use just the lowest order version because of its simplicity.

Accordingly, we have created code to take the partonic final state produced by DEDUCTOR, add the underlying event as just described, and write the resulting state, including the classical color string state  $\{c_f\}_N$ , to a “named pipe” that is sent to PYTHIA. This code is included in the sample user files for DEDUCTOR. We also include user code for PYTHIA that reads the information from DEDUCTOR, instructs PYTHIA to hadronize the partonic state, then analyzes the resulting hadronic state.

## B. Shower ordering variable

In DEDUCTOR, we order splittings according to decreasing values of a hardness parameter. The default choice of the hardness,  $\Lambda$ , is based on virtuality. For massless partons, the definition is

$$\begin{aligned}\Lambda^2 &= \frac{(\hat{p}_l + \hat{p}_{m+1})^2}{2p_l \cdot Q_0} Q_0^2 && \text{final state,} \\ \Lambda^2 &= \frac{|(\hat{p}_a - \hat{p}_{m+1})^2|}{2p_a \cdot Q_0} Q_0^2 && \text{initial state.}\end{aligned}\tag{1}$$

Here the mother parton in a final state splitting has momentum  $p_l$  and the daughters have momenta  $\hat{p}_l$  and  $\hat{p}_{m+1}$ . For an initial state splitting in hadron A, the mother parton has momentum  $p_a$ , the new (in backward evolution) initial state parton has momentum  $\hat{p}_a$  and the final state parton created in the splitting has momentum  $\hat{p}_{m+1}$ . We denote by  $Q_0$  a fixed vector equal to the total momentum of all of the final state partons just after the hard scattering that initiates the shower. The motivation for this choice is described in Ref. [10].

One can make other choices for the hardness variable. For instance, one can use the transverse momentum  $k_T = |\mathbf{k}_T|$  in the splitting. Transverse momentum is not a Lorentz invariant concept, so there are various definitions available. The definition used in DEDUCTOR is given in eqs. (B.10) and (A.8) of Ref. [13]:

$$\begin{aligned}\mathbf{k}_T^2 &= z(1-z)(\hat{p}_l - \hat{p}_{m+1})^2 && \text{final state,} \\ \mathbf{k}_T^2 &= (1-z)|(\hat{p}_a - \hat{p}_{m+1})^2| && \text{initial state.}\end{aligned}\tag{2}$$

We define the momentum fraction for a final state splitting by

$$\frac{\hat{p}_{m+1} \cdot \tilde{n}_l}{\hat{p}_l \cdot \tilde{n}_l} = \frac{1-z}{z},\tag{3}$$

where the auxiliary lightlike vector  $\tilde{n}_l$  is defined using the total momentum  $Q$  of all of the final state partons:

$$\tilde{n}_l = \frac{2p_l \cdot Q}{Q^2} Q - p_l.\tag{4}$$

For an initial state splitting,  $z$  is the ratio of momentum fractions before and after the splitting:

$$z = \frac{\eta_a}{\hat{\eta}_a} = \frac{p_a \cdot p_b}{\hat{p}_a \cdot p_b}.\tag{5}$$

We can change from  $\Lambda$  ordering to  $k_T$  ordering in DEDUCTOR. Doing that allows us to investigate the extent to which the choice of ordering variable really matters. With  $k_T$  ordering, the  $\mathbf{k}_T^2$  of each splitting is required to be smaller than the  $\mathbf{k}_T^2$  of the previous splitting. With  $\Lambda$  ordering, the

$\Lambda^2$  of each splitting is required to be smaller than the  $\Lambda^2$  of the previous splitting. In our numerical investigations in this paper, we look at jet production, which begins with a  $2 \rightarrow 2$  scattering that produces two partons with equal absolute values of transverse momenta,  $P_T^{\text{Born}}$ . The Born cross section is calculated with a factorization scale  $\mu_F^2$  and renormalization scale  $\mu_R^2$ . We set  $\mu_R^2 = \mu_F^2$  and

$$\mu_F = \frac{1}{\sqrt{2}} P_T^{\text{Born}} . \quad (6)$$

The motivation for this choice is that the next-to-leading order (NLO) one jet inclusive cross section is quite stable with respect changes in  $\mu_F^2$  near this point. We then need to choose the scale  $\mu_s^2$  at which the parton shower starts. With  $k_T$  ordering, the first splitting is required to satisfy  $k_T^2 < \mu_s^2$  where

$$\mu_s = P_T^{\text{Born}} \quad k_T \text{ ordering}. \quad (7)$$

With  $\Lambda$  ordering, the first splitting is required to satisfy  $\Lambda^2 < \mu_s^2$ , where we make a different choice for  $\mu_s$ . We recognize that the transverse momentum for the first splitting is intrinsically smaller than  $\Lambda^2$ :  $k_T^2 = (1-z)\Lambda^2$  for an initial state splitting or  $k_T^2 = z(1-z)\Lambda^2$  for a final state splitting. In either case,  $0 < (1-z) < 1$ . Thus,  $\Lambda^2$  for the first splitting is on average quite a lot larger than  $k_T^2$  for this splitting. Accordingly, we choose

$$\mu_s = \frac{3}{2} P_T^{\text{Born}} \quad \Lambda \text{ ordering}. \quad (8)$$

There is an additional requirement in the case of initial state splittings with  $\Lambda$  ordering. In successive initial state splittings, the factor  $2p_a \cdot Q_0$  in Eq. (1) can grow, so that successive virtualities  $|(\hat{p}_a - \hat{p}_{m+1})^2|$  can grow even while successive  $\Lambda^2$  values get smaller. We require that for each splitting,  $|k_T| < P_T^{\text{Born}}$ , where, as above,  $P_T^{\text{Born}}$  is the transverse momentum in the hard  $2 \rightarrow 2$  scattering that initiates the shower. In this way, we ensure that the hard scattering is indeed the hardest scattering in the whole event. This is discussed in Sec. 5.4 of Ref. [10], although we now replace Eq. (5.30) of Ref. [10] by  $|k_T| < P_T^{\text{Born}}$ .

### C. Threshold logarithms

We have presented a general analysis [4] of the structure of parton showers at any order of perturbation theory. In this treatment, there is a factor associated with the summation of threshold logarithms,

$$\mathcal{U}_{\mathcal{V}}(\mu_F^2, \mu_s^2) = \mathbb{T} \exp \left( \int_{\mu_F^2}^{\mu_s^2} \frac{d\mu^2}{\mu^2} \mathcal{S}_{\mathcal{V}}(\mu^2) \right) . \quad (9)$$

Here  $\mu^2$  is the hardness scale, which runs between the scale  $\mu_s^2$  at which the shower starts and the scale  $\mu_f^2$  at which the shower is stopped. The scale  $\mu_s^2$  is of the order of the scale of the hard interaction, while  $\mu_f^2$  is much smaller, typically of order 1 GeV<sup>2</sup>. The integrand is well behaved in the infrared, so that the integral is not sensitive to the value of  $\mu_f^2$ .

We included a summation of threshold logarithms in an earlier paper [13]. The important change between that treatment and the treatment of threshold logarithms in Ref. [4] lies in the fact that  $\mathcal{U}_V(\mu_f^2, \mu_s^2)$  in Eq. (11) is a single operator that acts on the state at the start of the shower. In Ref. [13], it was divided into smaller factors that acted on the states at intermediate stages of shower development. This led to an unphysical sensitivity to small scales, all the way down to the shower cutoff  $\mu_f^2$ . To avoid this, we inserted an *ad hoc* infrared cutoff into the threshold factors. The general analysis of Ref. [4] indicates that there should be a single threshold factor as in Eq. (9).

The operator  $\mathcal{S}_V(\mu^2)$  has an expansion to any order in  $\alpha_s$ . The notation of Ref. [4] is adapted to working to arbitrary perturbative order. For this paper, we need only its first order contribution,  $\mathcal{S}_V^{(1)}(\mu^2)$ . Since we want to work only to first order, it is most convenient to use the notation of Ref. [13] and previous DEDUCTOR papers [5–12] instead of the notation of Ref. [4]. In the notation of Ref. [13], the first order splitting operator  $\mathcal{H}_I(\mu^2)$  acts on a state  $|\rho\rangle$  with  $m$  final state partons and creates a state with  $m + 1$  final state partons. The inclusive probability associated with  $\mathcal{H}_I(\mu^2)|\rho\rangle$  is denoted  $(1|\mathcal{H}_I(\mu^2)|\rho)$ . There is another operator,  $\mathcal{V}(\mu^2)$ , that leaves the number of partons, their momenta and flavors unchanged. It is defined by integrating the parton spitting functions over the splitting variables  $z$  and  $\phi$ , so that

$$(1|\mathcal{V}(\mu^2)|\rho) = (1|\mathcal{H}_I(\mu^2)|\rho) \quad (10)$$

for any  $|\rho\rangle$ . This is the operator that, after approximations for color and spin, appears in the Sudakov exponent that comes between parton splittings.

When we evaluate  $\mathcal{S}_V(\mu^2)$  at order  $\alpha_s$  and use the notation of Ref. [13], the threshold operator in Eq. (9) is

$$\mathcal{U}_V(\mu_f^2, \mu_s^2) = \mathbb{T} \exp \left( \int_{\mu_f^2}^{\mu_s^2} \frac{d\mu^2}{\mu^2} [\mathcal{V}(\mu^2) - \{\mathcal{S}(\mu^2) - \mathcal{S}_{i\pi}(\mu^2)\}] \right). \quad (11)$$

Here the operator  $\mathcal{S}(\mu^2)$  has two contributions. One comes from the operator  $\mathcal{F}(\mu^2)$  that multiplies by the proper parton distribution functions to make a cross section. The derivative of  $\mathcal{F}(\mu^2)$  with respect to the scale contributes to  $\mathcal{S}(\mu^2)$ . There is also a contribution  $\mathcal{S}^{\text{pert}}(\mu^2)$  that comes from virtual graphs. The total is

$$\mathcal{S}(\mu^2) = \mathcal{S}^{\text{pert}}(\mu^2) - \mathcal{F}(\mu^2)^{-1} \left[ \mu^2 \frac{d}{d\mu^2} \mathcal{F}(\mu^2) \right]. \quad (12)$$

The operator  $\mathcal{S}^{\text{pert}}(\mu^2)$  has a contribution  $\mathcal{S}_{i\pi}(\mu^2)$  from the imaginary part of the one loop graphs. We remove this term. It belongs in the Sudakov exponent rather than the threshold factor because, although it changes parton colors, it preserves probabilities. We have, in fact, not included  $\mathcal{S}_{i\pi}(\mu^2)$  in the DEDUCTOR code used in this paper.

An exact treatment of leading threshold logarithms requires an exact treatment of color, which is available in the general formalism of Ref. [5]. The exact color treatment is not implemented in the code of DEDUCTOR. Rather, we are able to use only an approximation, the leading-color-plus (LC+) approximation [8]. The LC+ approximation consists of simply dropping some terms that appear in the exact color formulas.

We could simply use  $\mathcal{S}(\mu^2)$  and  $\mathcal{V}(\mu^2)$  as given in Ref. [13] to construct the threshold factor (11). However, we have found that some of the integrations that go into these operators can be performed so that they are accurate in a wider range of the kinematic variables compared to Ref. [13]. Thus we use the improved versions of  $\mathcal{S}(\mu^2)$  and  $\mathcal{V}(\mu^2)$  in DEDUCTOR v. 2.1.0. We explain the changes relative to Ref. [13] in Appendix A.

There is a factor associated with parton distribution functions that is related to the summation of threshold logarithms. DEDUCTOR begins with a Born color density matrix consisting of a sum of products of matrix elements  $|\mathcal{M}\rangle\langle\mathcal{M}|$  and parton factors

$$\text{pdf}[\text{LO}] = f_{a/A}^{\overline{\text{MS}},\text{NLO}}(\eta_a, \mu_F^2) f_{b/B}^{\overline{\text{MS}},\text{NLO}}(\eta_b, \mu_F^2). \quad (13)$$

For this paper, we use the CT14 NLO parton distributions [60]. Then with a “standard” shower (std.) we apply a probability preserving shower, still starting with the same parton factor:

$$\text{pdf}[\text{std.}] = f_{a/A}^{\overline{\text{MS}},\text{NLO}}(\eta_a, \mu_F^2) f_{b/B}^{\overline{\text{MS}},\text{NLO}}(\eta_b, \mu_F^2). \quad (14)$$

The shower splitting functions use parton distribution functions  $f_{a/A}(\eta_a, \mu^2)$  and  $f_{b/B}(\eta_b, \mu^2)$  that are adapted to the definition of the parton shower. These are described in Ref. [4] and in Ref. [13]. With  $k_T$  ordering,  $f_{a/A}(\eta_a, \mu^2)$  and  $f_{b/B}(\eta_b, \mu^2)$  are just  $\overline{\text{MS}}$  parton distribution functions with leading order evolution,  $f_{a/A}^{\overline{\text{MS}},\text{LO}}(\eta_a, \mu^2)$ .<sup>2</sup> With  $\Lambda$  ordering, there is a substantial difference between  $f_{a/A}(\eta_a, \mu^2)$  and  $f_{a/A}^{\overline{\text{MS}},\text{LO}}(\eta_a, \mu^2)$ . We define all of these parton distribution functions to agree at a low scale  $\mu_F^2$ . (See Appendix B of Ref. [4] and Sec. 4.1 of Ref. [13].) They differ in their evolution equations.

---

<sup>2</sup> There is a small difference that arises from the fact that in the dimensionally regulated definition of the  $\overline{\text{MS}}$  parton distribution functions, a gluon has  $2 - 2\epsilon$  polarization states instead of 2 polarization states. See Appendix B of Ref. [4]. We ignore this difference in this paper.

The full result (full) given by DEDUCTOR includes the factor  $\mathcal{U}_V(\mu_F^2, \mu_S^2)$  from Eq. (11) and a modified parton factor,

$$\text{pdf}[\text{full}] = Z_a Z_b f_{a/A}^{\overline{\text{MS}},\text{NLO}}(\eta_a, \mu_F^2) f_{b/B}^{\overline{\text{MS}},\text{NLO}}(\eta_b, \mu_F^2). \quad (15)$$

where

$$Z_a = \frac{f_{a/A}(\eta_a, \mu_S^2)}{f_{a/A}^{\overline{\text{MS}},\text{LO}}(\eta_a, \mu_S^2)}, \quad Z_b = \frac{f_{b/B}(\eta_b, \mu_S^2)}{f_{b/B}^{\overline{\text{MS}},\text{LO}}(\eta_b, \mu_S^2)}. \quad (16)$$

To a good approximation, the  $\overline{\text{MS}}$  parton distribution functions cancel in pdf[full], leaving just  $f_{a/A}(\eta_a, \mu_S^2) f_{b/B}(\eta_b, \mu_S^2)$ . However, this cancellation is not exact because we define the denominators in  $Z_a$  and  $Z_b$  at a scale  $\mu_S^2$  and with just lowest order evolution so that it matches the numerator except for the change of evolution kernels.

The factor  $Z_a Z_b$  equals 1 with  $k_T$  ordering, but it can be substantially larger than 1 with  $\Lambda$  ordering. It is part of the summation of threshold logarithms, as described in Secs. 4.2 and 9.4 of Ref. [13].

### III. NUMERICAL RESULTS

In this section, we use the new version of DEDUCTOR to address questions in jet physics.

#### A. One jet inclusive cross section

We begin with the one jet inclusive cross section  $d\sigma/dP_T$  as calculated in DEDUCTOR with  $\Lambda$  ordering for jets with  $|y_{\text{jet}}| < 2$  for the LHC at 13 TeV. We use CT14 NLO parton distributions [60]. The jets are defined with the anti- $k_T$  algorithm [61, 62] with  $R = 0.4$ . We set the renormalization and factorization scale in the hard cross section to  $\mu_R = \mu_F = P_T/\sqrt{2}$ .

DEDUCTOR starts with the Born cross section for two jet production. It would, of course, be best to put in the right NLO matrix elements and subtractions to make match the shower to the NLO jet cross section [63–83]. In principle, this is straightforward in the DEDUCTOR framework [4]. However, we have not developed the code to do this. Thus the parton shower needs to do as good a job as possible to calculate the cross section accurately. For this purpose, it is important to include the threshold factors  $\mathcal{U}_V(\mu_F^2, \mu_S^2)$ , Eq. (9), and  $Z_a Z_b$ , Eq. (16), and to make a sensible choice for the starting scale  $\mu_S$  of the shower. We use Eq. (8) for  $\mu_S$  in the default  $\Lambda$  ordered shower.

In DEDUCTOR, we use the LC+ approximation for color, with the maximum color suppression index, as defined in Ref. [8], set to 4. This means that contributions suppressed by more than

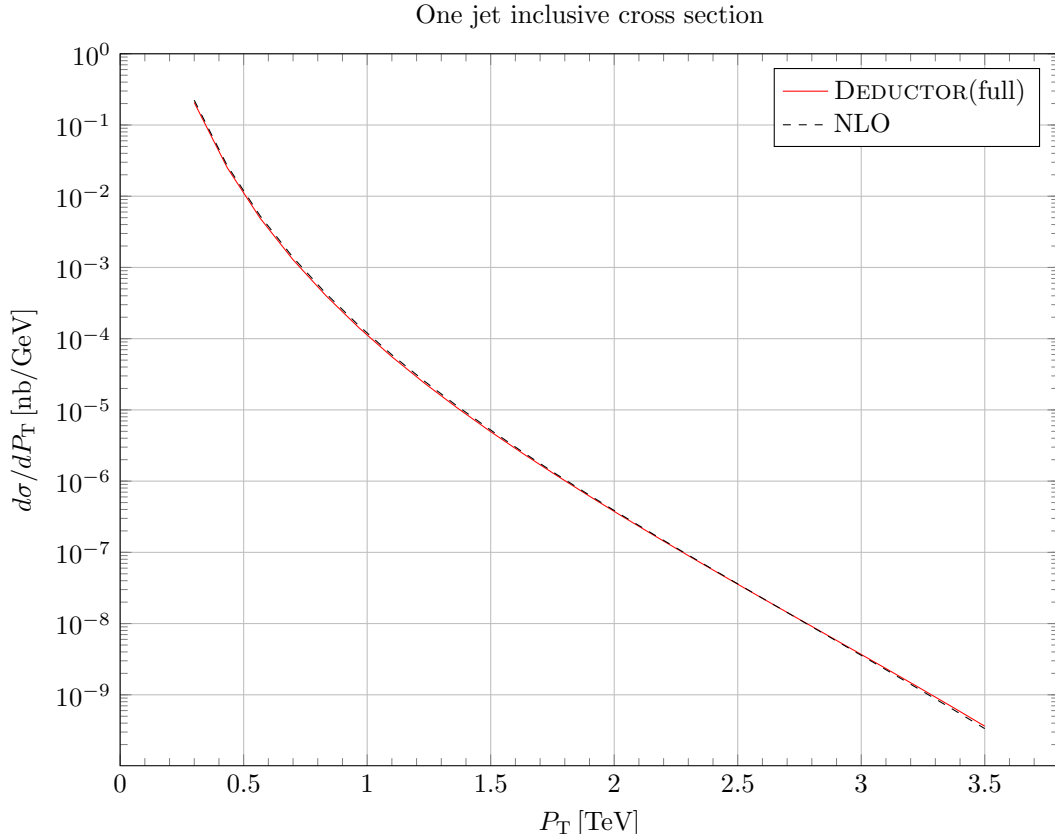


FIG. 1. One jet inclusive cross section  $d\sigma/dP_T$  for the production of a jet with transverse momentum  $P_T$  and rapidity in the range  $-2 < y < 2$ . The cross section is for the LHC at 13 TeV. We use the anti- $k_T$  algorithm [61] with  $R = 0.4$ . The solid red curve is  $d\sigma(\text{full})/dP_T$ , obtained with threshold effects. The dashed black curve is an NLO calculation [84].

$1/N_c^4$  are dropped. Note, however, that only some, but not all, of the terms proportional to  $1/N_c^2$  and  $1/N_c^4$  are retained in the LC+ approximation.

We show the DEDUCTOR result for  $d\sigma(\text{full})/dP_T$  as the solid red curve in Fig. 1. Here “full” refers the calculation including all contributions. We also show, as a black dashed curve, the purely perturbative NLO cross section [84] with the same parton distribution functions and scale choices. We see that the parton shower calculation matches the NLO calculation reasonably well.

In the following subsections, we will examine the jet cross section in more detail. Since it is not easy to see details in a plot like that in Fig. 1 in which the cross section falls by nine orders of magnitude, we will show ratios of calculated cross sections as functions of  $P_T$ .

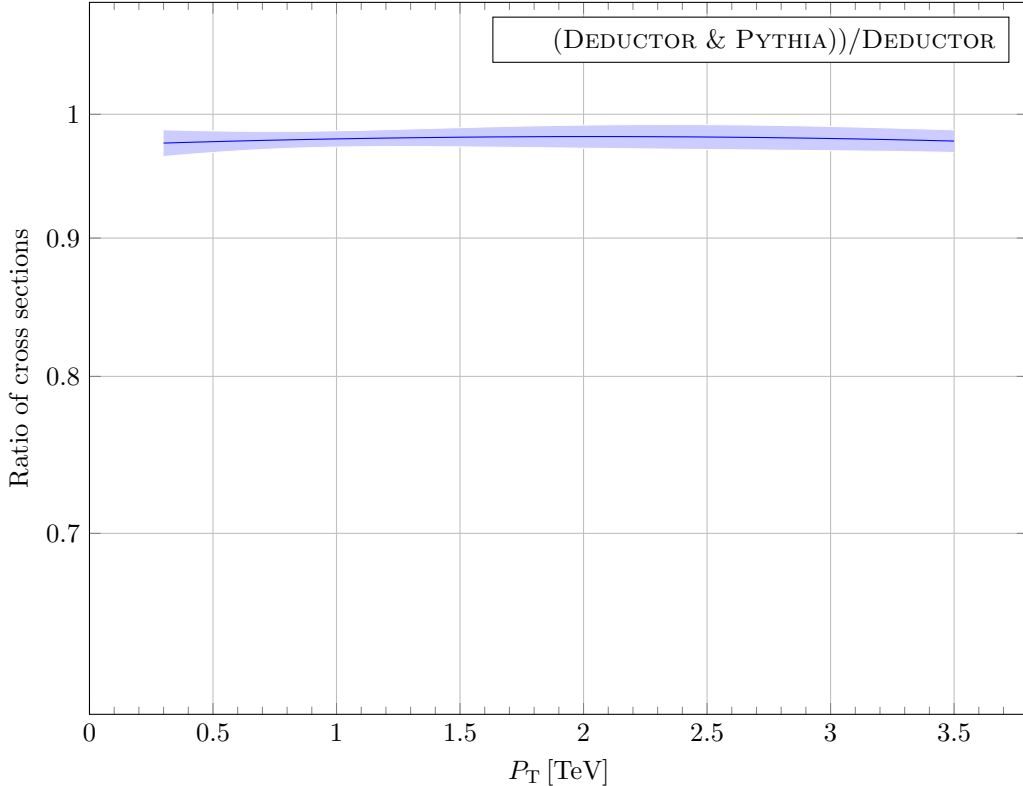


FIG. 2. Ratio of the one jet inclusive cross section  $d\sigma/dP_T$  calculated by DEDUCTOR with an underlying event and with hadronization by PYTHIA to the same cross section calculated by DEDUCTOR with no non-perturbative input.

### B. Underlying event and hadronization

The DEDUCTOR results presented above represent a purely perturbative parton shower, with an infrared cutoff at around a 1 GeV scale for the transverse momentum of splittings. One can wonder whether nonperturbative effects from an underlying event or hadronization can significantly affect the jet cross section.

We include an underlying event using the simple model described in Sec. II A and then let PYTHIA hadronize the event as also described in Sec. II A. In Fig. 2, we show the ratio of the jet cross section  $d\sigma/dP_T$  calculated with an underlying event and hadronization to the same cross section calculated at the parton level. We use the anti- $k_T$  jet algorithm with  $R = 0.4$ . We see that the underlying event and hadronization changes the cross section by only about 2%. This is a small effect, so in the remainder of this section we work only at the partonic level.

### C. Effect of jet finding

The intuitive picture of a jet is that it is a parton created in a hard interaction. However, this picture does not closely match reality, as we can see by simulating reality with a parton shower. At the Born level, one has just two final state partons, with  $\mathbf{p}_{T,1} = -\mathbf{p}_{T,2}$ . After showering, we have many final state partons, which are grouped into jets. The jet  $P_T$  is typically quiet close to  $|\mathbf{p}_{T,1}|$ . However, it can be larger if a parton from an initial state splitting enters the jet. It can be smaller if a parton from a final state splitting leaves the jet. Additionally,  $P_T$  can be either larger or smaller than  $|\mathbf{p}_{T,1}|$  if the jet recoils against an initial state emission. These effects have the potential to substantially change the cross section because the cross section falls very steeply as a function of  $P_T$ .

We can examine this effect in DEDUCTOR by turning off the threshold factor. We call the resulting cross section  $d\sigma(\text{std.})/dP_T$  because it is the result of a standard probability preserving shower. Then we look at the ratio to the Born cross section,  $d\sigma(\text{LO})/dP_T$ :

$$r(P_T) = \frac{d\sigma(\text{std.})/dP_T}{d\sigma(\text{LO})/dP_T}. \quad (17)$$

In this section, we use the anti- $k_T$  jet algorithm with  $R = 0.4$ . We can do the same thing using the parton level showering produced by PYTHIA and DIRE. Here, there is no threshold factor to turn off. We choose  $\mu_F = \mu_R = P_T/\sqrt{2}$  at the level of the hard scattering and use CT14 NLO parton distributions in each case. For other parameters, we use the default choices in PYTHIA and DIRE. For DEDUCTOR, we use the parameters from Sec. III A.

We exhibit  $r(P_T)$  for DEDUCTOR, PYTHIA, and DIRE in Fig. 3. We can make three observations. First, the three shower programs give substantially different results for  $r(p_T)$ . Second,  $r(p_T)$  for DEDUCTOR and, to a lesser extent for DIRE, is substantially smaller than 1. Third, there is some dependence on  $p_T$ , but it is not large. One would expect that the effect of the jet algorithm would depend on the value of  $R$ : for smaller  $R$ , it should be much easier for partons to be radiated out of the jet, so that  $r(P_T)$  should be smaller. To investigate this, we exhibit in Fig. 4 the same plot for  $R = 0.2$  and  $R = 0.7$ . We see that, indeed, for smaller  $R$ ,  $r(P_T)$  is indeed smaller, while  $r(P_T)$  is larger for larger  $R$ . In fact, according to DIRE,  $r(P_T)$  is close to 1 for  $R = 0.7$  while according to PYTHIA,  $r(P_T)$  is greater than 1 for  $R = 0.7$ .

We can explore the difference among the three parton showers by plotting  $r(2 \text{ TeV})$  versus  $\log(1/R)$ . We see that all three programs give approximately straight lines in this plot. We see also that the slopes as determined from the  $R = 0.4$  and  $R = 0.2$  points are not very different

among the three programs. This is to be expected since the slopes  $dr(P_T)/d\log(1/R)$  are given rather directly by perturbation theory [85–87]. We also note that the three programs give very different results at fixed  $R$ , for instance at  $R = 0.4$ .

Why do the three programs give different results at  $R = 0.4$ ? We can get some idea by calculating a function  $f(z)$  that gives an effective distribution of jets in a parton as a function of the ratio of the jet  $P_T$  to the parton  $p_T$ . For a theoretical analysis of  $f(z)$  see Ref. [87]. In nature, of course, we do not have access to the parton that initiates a jet, but in a parton shower program, we do. Each event starts with a Born level  $2 \rightarrow 2$  scattering that produces two final state partons with  $\mathbf{p}_{T,1} = -\mathbf{p}_{T,2}$ . We define  $P_T^{\text{Born}} = |\mathbf{p}_{T,1}|$ . We select events in which the two initiating partons have  $P_T^{\text{Born}}$  close to 3 TeV,  $2.8 \text{ TeV} < P_T < 3.3 \text{ TeV}$ , and for which  $|y_1| < 2$  and  $|y_2| < 2$ . For these events, we look at the final state after showering. We look at all final state jets with rapidity  $|y| < 2$  and transverse momentum  $P_T$  and define

$$z = \frac{P_T}{P_T^{\text{Born}}}. \quad (18)$$

Then we define  $f(z) dz$  to be the ratio of the number of final state jets in a range  $dz$  to the number of Born level partons in the sample, which is twice the number of events in the sample. We display  $f(z)$  in Fig. 6. For  $z > 1.01$ , we see that  $f(z)$  for DIRE (in black) and DEDUCTOR (in red) are close to each other while  $f(z)$  for PYTHIA (in blue) is larger. With a steeply falling  $P_T$  spectrum, this increases the PYTHIA after-showering cross section. It may be surprising to have jets with more transverse momentum than the initiating parton, but it can easily happen. When there is a parton emitted from the initial state, the two original partons recoil in the opposite direction in order for transverse momentum to be conserved. Thus an initial state emission in the direction opposite to the observed jet increases the transverse momentum of the jet.<sup>3</sup> It appears that this effect is bigger in PYTHIA than in DIRE or DEDUCTOR.

For  $z < 0.99$ ,  $f(z)$  for PYTHIA and for DIRE are close to each other while  $f(z)$  for DEDUCTOR is larger. It seems plausible that this happens because DEDUCTOR has more final state radiation out of the jet. More radiation out of the jet makes  $f(z)$  larger for  $z < 1$ . Here the cone size,  $R = 0.4$  is not particularly small, so this is wide angle radiation. To see how this happens in more detail,

---

<sup>3</sup> We thank Gavin Salam for this observation.

we fit  $f(z)$  according to PYTHIA, DIRE, and DEDUCTOR in the range  $0.8 < z < 0.97$ :

$$\begin{aligned}
f(z; \text{PYTHIA}) &\approx 2.10 \frac{1 - 0.9}{1 - z} - 1.61 \frac{\log(1 - z)}{\log(1 - 0.9)} - 0.41 , \\
f(z; \text{DIRE}) &\approx 1.82 \frac{1 - 0.9}{1 - z} - 0.41 \frac{\log(1 - z)}{\log(1 - 0.9)} - 0.10 , \\
f(z; \text{DEDUCTOR}) &\approx 1.91 \frac{1 - 0.9}{1 - z} + 0.61 \frac{\log(1 - z)}{\log(1 - 0.9)} - 0.53 .
\end{aligned}
\tag{19}$$

In each case, we find that around  $z = 0.9$ ,  $f(z)$  is dominated by a term proportional to  $1/(1 - z)$ . This is expected from the  $1/(1 - z)$  singularity from soft gluon emissions. In each case, there is also a term with a weak  $\log(1 - z)$  singularity and a constant term. The coefficient of the  $1/(1 - z)$  leading singularity for DEDUCTOR lies between the corresponding coefficients for PYTHIA and DIRE, but the differences are small. To a good approximation, the differences between  $f(z)$  for DEDUCTOR and DIRE or PYTHIA have only a constant term and a  $\log(1 - z)$  term. It is not a surprise that there are differences between DEDUCTOR splitting and DIRE or PYTHIA splitting that are only weakly singular. The DEDUCTOR splitting kernel has contributions corresponding to soft interference diagrams in an eikonal approximation and then “direct” terms whose collinear limit is the DGLAP evolution kernel. However, the direct terms are not obtained from the DGLAP kernel but are rather designed to approximate as closely as possible the Feynman diagrams from which the DGLAP kernel is derived [5]. On the other hand, DIRE and PYTHIA are based more closely on the DGLAP kernel.

It is good to understand the differences between the three results Fig. 6, but it is important to appreciate also their similarities. In each case, we have a function that is strongly peaked near  $z = 1$ . The rather small differences in  $f(z)$  lead to substantial differences in  $d\sigma/dP_T$  because the cross section falls so steeply with  $P_T$ .

#### D. Effect of the threshold factors

The threshold factors  $\mathcal{U}_\gamma(\mu_f^2, \mu_s^2)$  from Eq. (11) and  $Z_a Z_b$  from Eq. (16) are included in DEDUCTOR. A factor similar to  $\mathcal{U}_\gamma(\mu_f^2, \mu_s^2)$  was included in an earlier version of DEDUCTOR that we used for Ref. [13]. However, in this version we did not have the general results of Ref. [4] and consequently did not have the proper organization for the threshold effect. As a result, the threshold effects were contaminated by soft scale physics. To eliminate this contamination, we had to use an *ad hoc* infrared regulator. With the organization from Ref. [4], we have a single factor in which the integral over  $\mu^2$  in Eq. (11) is well behaved in the infrared, so that no regulator is needed.

Effect of jet finding,  $R = 0.4$

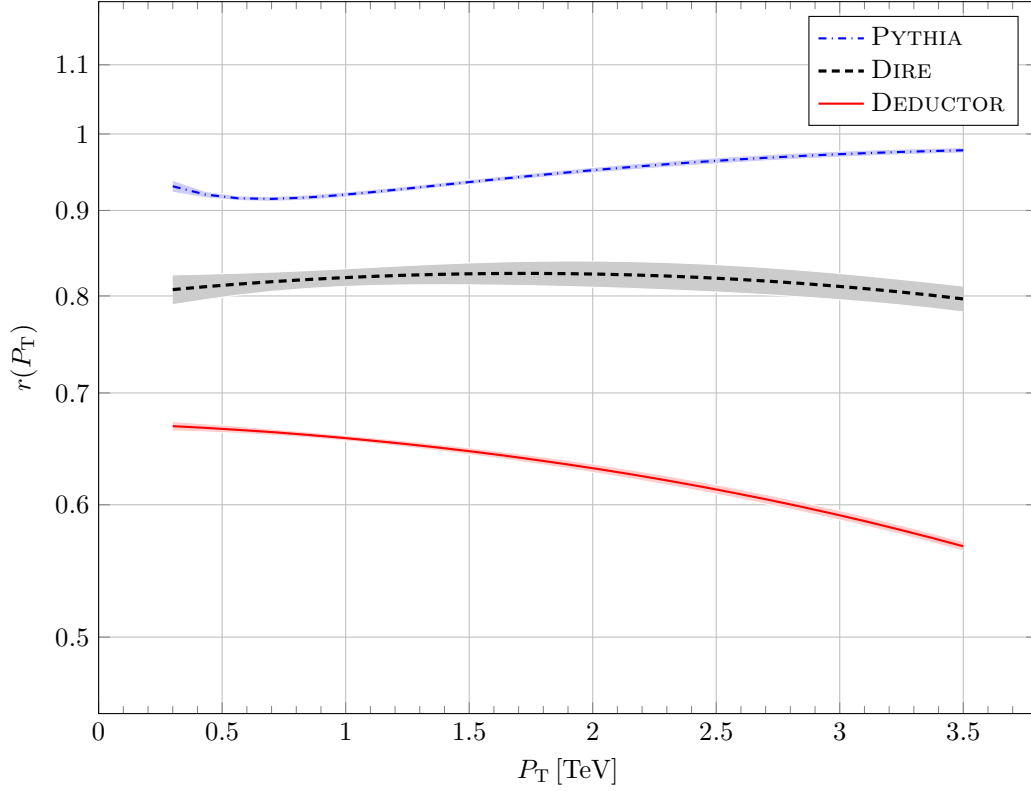


FIG. 3. Ratio  $r(P_T)$  of the one jet inclusive cross section  $d\sigma/dP_T$  calculated after showering to the cross section at the Born level according to (from top to bottom) PYTHIA, DIRE, and DEDUCTOR.

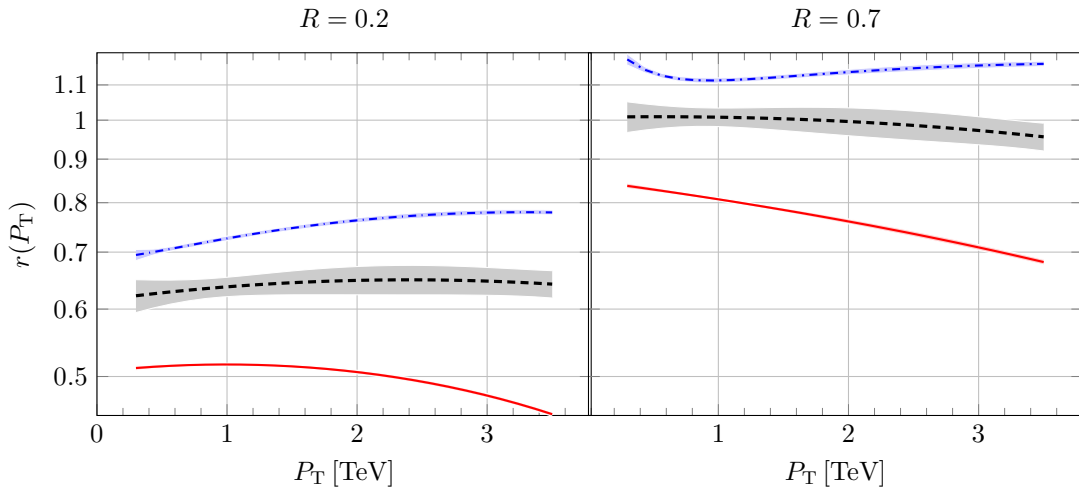


FIG. 4. Ratio  $r(P_T)$  of the one jet inclusive cross section  $d\sigma/dP_T$  calculated after showering to the cross section at the Born level for  $R = 0.2$  and for  $R = 0.7$ . The labelling is the same as in Fig. 3.

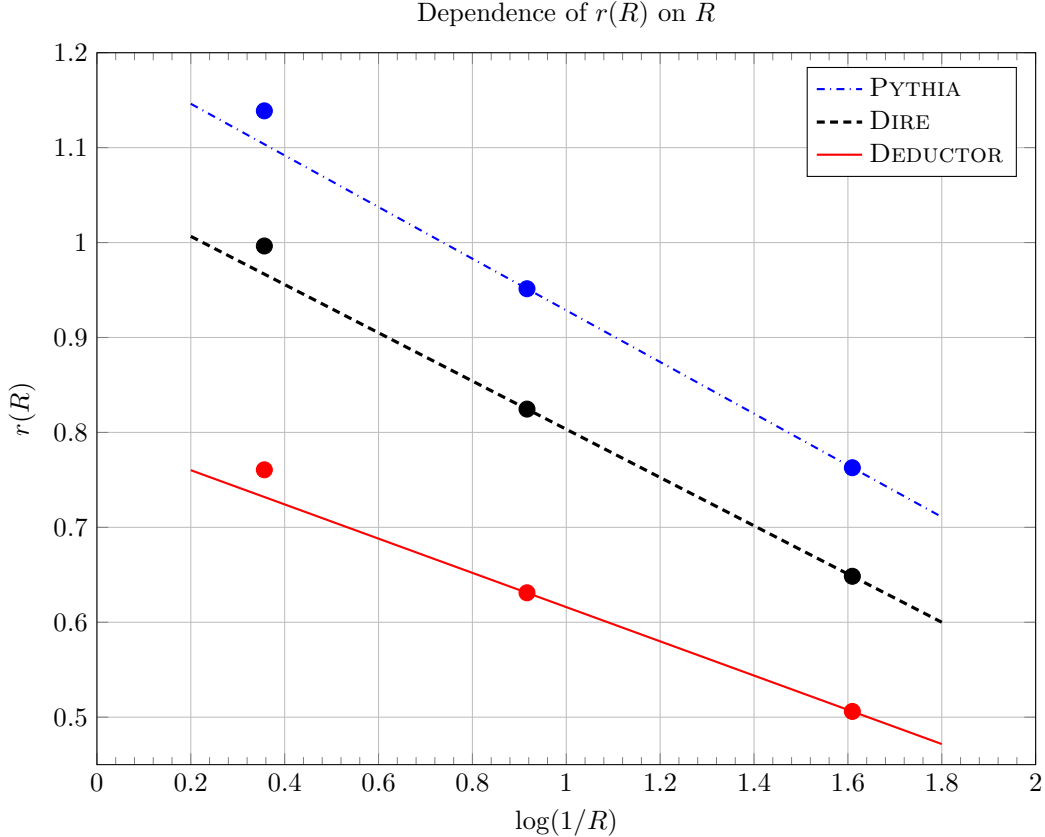


FIG. 5. Ratio of the one jet inclusive cross section  $d\sigma/dP_T$  calculated after showering to the cross section at the Born level at  $P_T = 2$  TeV versus  $\log(1/R)$  for (from top to bottom) PYTHIA, DIRE, and DEDUCTOR.

In this subsection, we examine the effect of the threshold factors. We look first at the inclusive jet cross section with  $R = 0.4$  calculated with DEDUCTOR with  $\Lambda$  ordering using the parameters from Sec. III A. In Fig. 7, we plot ratios  $K$  of the cross sections calculated with various approximations “A” to the purely perturbative NLO cross section,

$$K(\text{“A”}) = \frac{d\sigma(\text{“A”})/dP_T}{d\sigma(\text{NLO})/dP_T}. \quad (20)$$

First, in black (dashed), we plot  $K(\text{LO})$  using the Born cross section in the numerator. We see that  $K(\text{LO})$  is rather close to 1. That is, with the choice of  $\mu_R^2$  and  $\mu_F^2$  that we use, the LO cross section is fairly close to the NLO cross section.

Next, in blue, we plot  $K(\text{std.})$  using DEDUCTOR with the threshold factors turned off, so that we have a standard probability preserving parton shower. Showering reduces the cross section substantially, multiplying it by a factor of roughly 0.6. This is the effect that we examined in section III C.

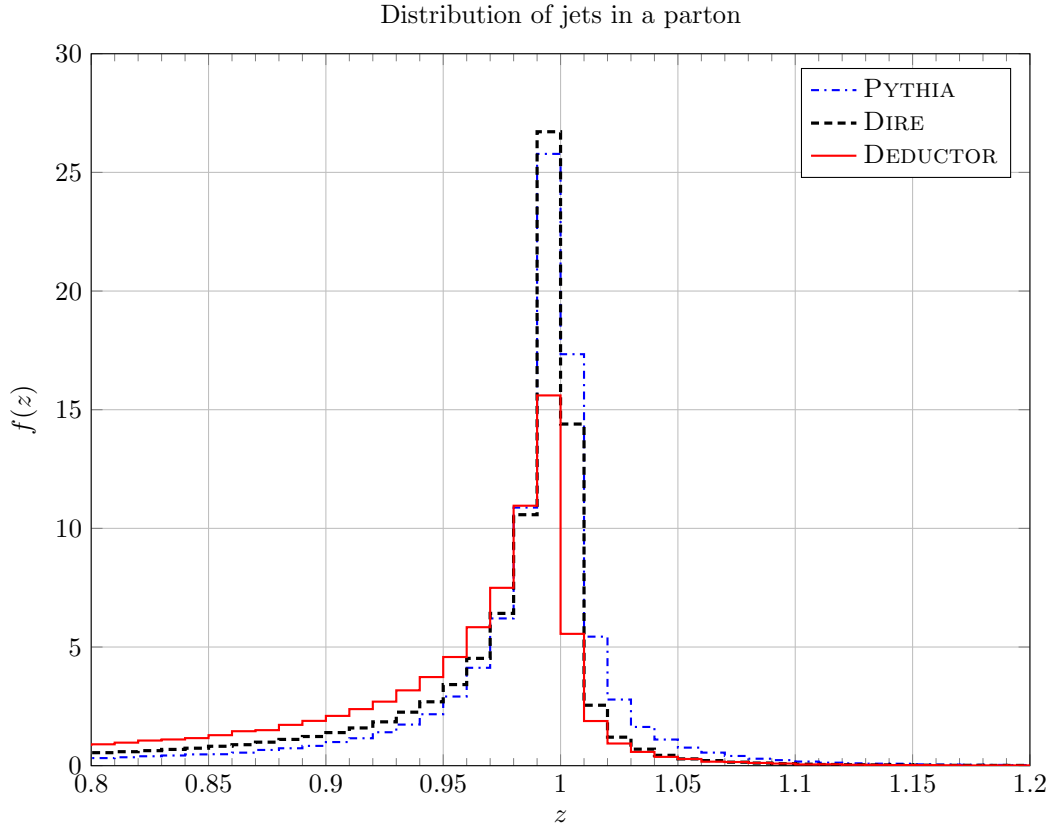


FIG. 6. Effective distribution of jets in a parton,  $f(z)$  for PYTHIA, DIRE, and DEDUCTOR for  $R = 0.4$  jets with  $P_T \approx 2$  TeV.

Next, in red, we plot  $K(\text{full})$  using DEDUCTOR including the threshold factors. We see that the threshold factors increase the cross section by a factor that ranges from about 1.3 at  $P_T = 0.3$  TeV to more than 2 at  $P_T = 3.5$  TeV. With both showering and the threshold factors included, the full cross section is quite close to what one gets with an NLO calculation.

There is a calculation of de Florian, Hinderer, Mukherjee, Ringer and Vogelsang (FHMRV) [41] that is relevant to this analysis. This calculation sums threshold logarithms and also the logarithms of  $1/R$  that arise from the jet definition. These authors then expand the analytic result perturbatively to either NLO or NNLO. We show as a green dash-dotted line the ratio  $K(\text{FHMRV NLO})$  from this calculation expanded to NLO. We note that this result is pretty close to the purely perturbative NLO result. We also show as a purple dashdotted line the ratio  $K(\text{FHMRV NNLO})$  corresponding to the NNLO calculation. It is puzzling to us that  $K(\text{FHMRV NNLO})$  decreases with increasing  $P_T$ .

How do these results depend on the cone size? In Fig. 8, we show the results for  $R = 0.2$  on the

left and for  $R = 0.7$  on the right. We see that for  $R = 0.2$  there is a bigger drop going from the LO cross section to the std. cross section, while for  $R = 0.7$  the drop is smaller. This is the effect that we investigated in Sec. III C. On the other hand, the threshold factors that take us from the std. result to the full result are independent of  $R$ . In the end, the full DEDUCTOR cross section is fairly close to the NLO cross section.

How do the results depend on the choice of ordering variable for the shower? In the results presented above, we used  $\Lambda$ , Eq. (1), as the ordering variable. This is the default in DEDUCTOR. However, we can choose  $k_T$ , Eq. (2). Then instead of Fig. 7 we get Fig. 9. The DEDUCTOR(std.) result is modified a little. The main difference is that with  $k_T$  ordering, the threshold effect is quite a lot smaller at large  $P_T$  than with  $\Lambda$  ordering. The result is that the DEDUCTOR(full) result is 30% smaller than with  $\Lambda$  ordering.

We believe that we can draw two robust conclusions from these results. First, the effect of applying the jet definition to the partons emerging from the hard scattering is substantial. Second, the threshold effects are substantial. These substantial effects act in opposite directions, so that they tend to cancel each other out. That is, the perturbative calculation of  $d\sigma/dp_T$  beyond lowest order involves large effects that tend to cancel. These cancellations appear at all orders of perturbation theory. In particular, they occur within the NLO calculation. Thus, the NLO calculation is more delicate than is at first apparent.

### E. Gaps between jets

Consider an event with two high- $P_T$  jets that are separated by a large difference  $\Delta y$  in rapidity. We can define a gap fraction  $f$  to be the ratio of the cross section to produce the two jets to the cross section to produce the two jets and produce no more jets with transverse momenta above some cutoff  $p_T^{\text{cut}}$  in the rapidity interval between the two high- $P_T$  jets. It is of some importance to understand the gap fraction  $f$  because it is often useful in experimental investigations to impose a requirement that there be some minimum number of high  $p_T$  jets in an event but no jets beyond this that have  $p_T$  greater than some value  $p_T^{\text{cut}}$ .

In addition, the behavior of  $f$  as a function of how the gap is defined is a matter of substantial theoretical interest because it brings together several issues concerning the structure of QCD. Many of these issues are reviewed in Ref. [88]. At a first level in an analytic summation of leading logarithms [89, 90], one uses the exponential of a Sudakov exponent constructed from one loop graphs for the virtual exchange of a low transverse momentum gluon. There are further subtleties

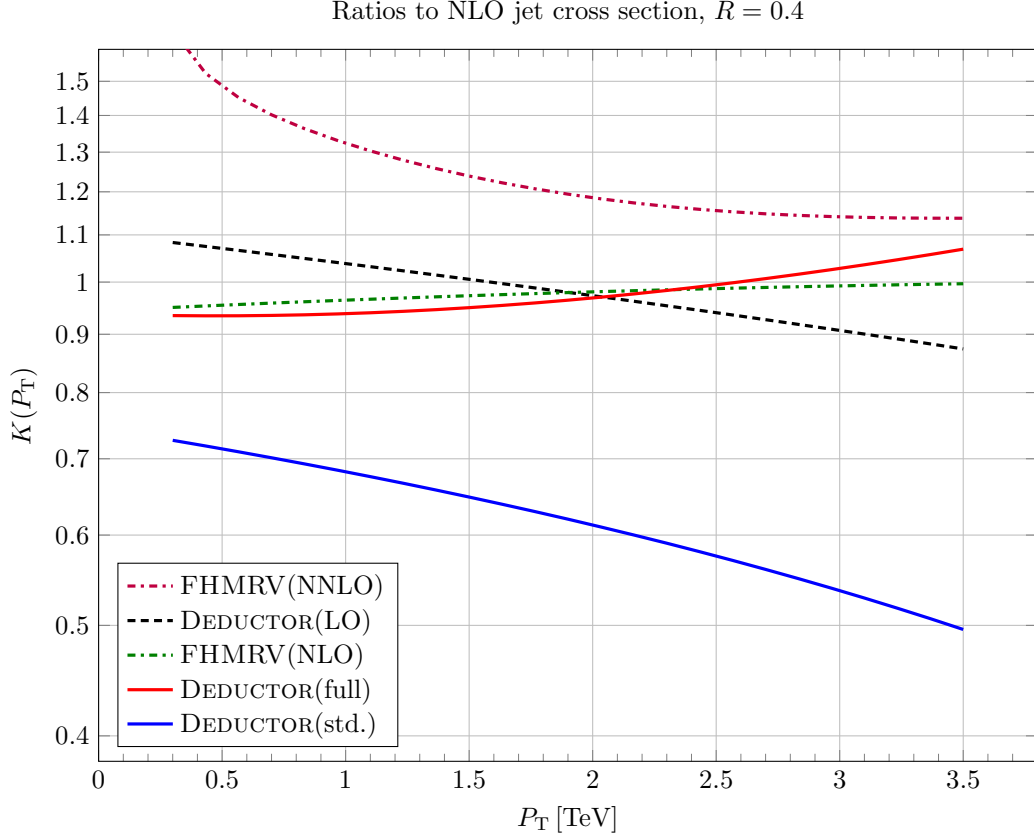


FIG. 7. Ratios  $K(P_T)$  of the one jet inclusive cross section  $d\sigma/dP_T$  to the NLO cross section calculated in different approximations. The curves are ordered as in the legend at  $P_T = 1$  TeV.

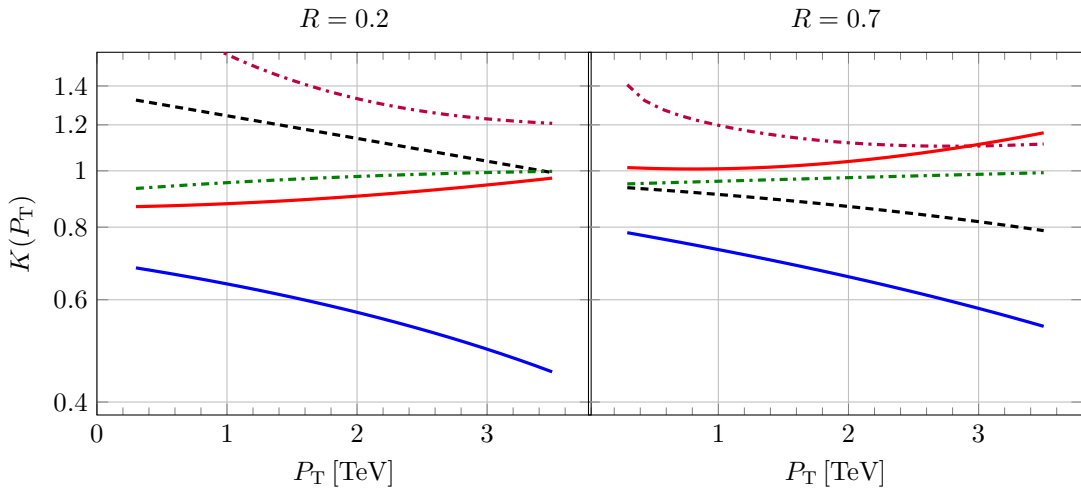


FIG. 8. Ratios  $K(P_T)$  of the one jet inclusive cross section  $d\sigma/dP_T$  to the NLO cross section with  $R = 0.2$  and  $R = 0.7$ . The labelling is the same as in Fig. 7.

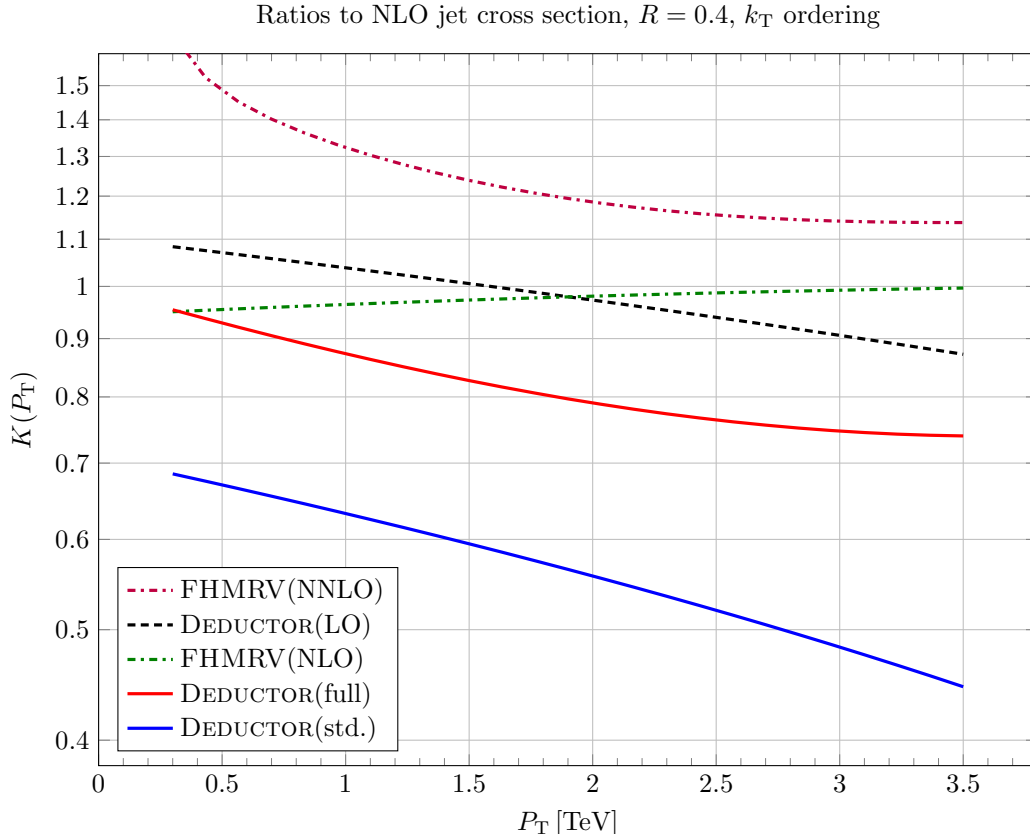


FIG. 9. Ratios  $K(P_T)$  of the one jet inclusive cross section  $d\sigma/dP_T$  to the NLO cross section calculated using DEDUCTOR in different approximations with  $k_T$  ordering. The FHMRV curves are the same as in Fig. 7.

in the analytic treatment. When the rapidity separation  $\Delta y$  between the leading jets is large, factors of  $\Delta y$  in the exponent are especially important [91]. There can also be “non-global” logarithms with a different structure than seen in the simplest analytic treatment [92–95]. Furthermore, some of these logarithms are “super-leading” in the sense of having more powers of logarithms per power of  $\alpha_s$  than one gets in the simple analysis [88, 96–98].

We will compare to results from Atlas [99]. In the Atlas results,  $p_T^{\text{cut}}$  is fixed and the gap fraction  $f$  is plotted as a function of the transverse momentum of the hard jets. Specifically, Atlas uses a data sample at  $\sqrt{s} = 7$  TeV. Jets are defined using the anti- $k_T$  algorithm [61] with  $R = 0.6$ . All jets in the rapidity window  $-4.4 < y < 4.4$  are considered if they have  $p_T > p_T^{\text{cut}} = 20$  GeV. Of these jets, the two jets with the highest  $p_T$  are selected. Of the two leading jets, let jet 1 have the highest rapidity and let jet 2 have the lowest rapidity. The event is characterized by the rapidity difference  $\Delta y = y_1 - y_2$  and the average transverse momentum  $\bar{p}_T = (p_{T,1} + p_{T,2})/2$ . The event

has a gap if there is no jet (with  $p_T > p_T^{\text{cut}}$ ) in the rapidity range  $y_1 < y < y_2$ . Only a fraction  $f$  of events with a given  $\Delta y$  and  $\bar{p}_T$  has a gap.

There are a number of comparisons of the Atlas data to theory. Of these, we mention the approach in Ref. [100], which looks for places in which the summation of  $\Delta y$  factors are important. The paper [101] uses  $\alpha_s^2 + \alpha_s^3$  perturbation theory matched to the SHERPA parton shower, obtaining a good match to the data.

We will use DEDUCTOR, but also compare to purely perturbative results. We write the gap fraction in the form

$$f(\bar{p}_T, \Delta y) = 1 - \frac{d\sigma_3/[d\bar{p}_T d\Delta y]}{d\sigma_2/[d\bar{p}_T d\Delta y]}. \quad (21)$$

Here  $d\sigma_2/[d\bar{p}_T d\Delta y]$  is the cross section to produce at least two jets in the rapidity window  $-4.4 < y < 4.4$  such that the two jets in the rapidity window with the largest  $p_T$  satisfy  $\bar{p}_T = (p_{T,1} + p_{T,2})/2$  and  $\Delta y = |y_1 - y_2|$ . This is an infrared safe jet cross section for which the lowest order contribution has two partons in the final state. We calculate this cross section at NLO using NLOJET++ [102]. In the numerator,  $d\sigma_3/[d\bar{p}_T d\Delta y]$  is the cross section to produce at least three jets in the rapidity window  $-4.4 < y < 4.4$  such that the two jets in the rapidity window with the largest  $p_T$  satisfy  $\bar{p}_T = (p_{T,1} + p_{T,2})/2$  and  $\Delta y = |y_1 - y_2|$  and such that there is a third jet with  $\min(y_1, y_2) < y_3 < \max(y_1, y_2)$  and  $p_{T,3} > p_T^{\text{cut}}$ . This is an infrared safe jet cross section for which the lowest order contribution has three partons in the final state. Again, we calculate this cross section at NLO using NLOJET++.

A similar calculation was carried out in Ref. [103]. In this calculation,  $f(\bar{p}_T, \Delta y)$  was expanded in powers of  $\alpha_s$  and only the  $\alpha_s^1$  and  $\alpha_s^2$  terms were retained. The outcome was that for  $\Delta y > 3$  the perturbative result became unstable and could not come close to the experimental result. Our approach is to keep the numerator and the denominator in Eq. (21) as units that each represent sensible physical cross sections and should not be disassembled.<sup>4</sup> Nevertheless, given that there are large logarithms in this problem, one may expect that the perturbative formula in Eq. (21) will fail to match experiment.

For the purpose of capturing the effects seen in analytical summations of logarithms, there may be an advantage to using a parton shower approach in place of analytical summations since, in principle, a parton shower can trace complex patterns involving the emission of real gluons and the subsequent virtual exchanges between these gluons. However, a better treatment of color within the shower is needed to realize this potential advantage. Furthermore, the analytic treatments

---

<sup>4</sup> Thus we use the 1/1 Padé approximant for  $f/\alpha_s$  instead of the 1/0 Padé approximant.

suggest that exponentiated logarithms of  $\Delta y$  are crucial. This suggests that a rapidity-ordered treatment might be desirable, as in Ref. [100]. We do not have a rapidity ordered shower, but we can choose  $\Lambda$  ordering or  $k_T$  ordering. What can happen is not completely intuitive. For instance, suppose that the Born hard scattering produces partons 1 and 2 with  $0 = \mathbf{p}_{T,1}^{\text{Born}} + \mathbf{p}_{T,2}^{\text{Born}}$ . Then an initial state emission can produce parton 3. But partons 1 and 2 must then recoil against parton 3 so that in the new state  $0 = \mathbf{p}_{T,1} + \mathbf{p}_{T,2} + \mathbf{p}_{T,3}$ . Then it is possible that partons 1 and 3 are the highest  $P_T$  jets in the final state and a somewhat softer parton 2 lies in the gap between partons 1 and 3. It can also happen that parton 3 is created in a soft, wide angle emission and is the smallest  $P_T$  jet and, furthermore, lies in the gap between partons 1 and 2. It can also happen that  $\Lambda$  ordering can give one shower history, say  $(1, 2) \rightarrow (1, 2, 3)$  while  $k_T$  ordering can give a different shower history for the same parton momenta, say  $(1, 3) \rightarrow (1, 2, 3)$ . Then the same state  $(1, 2, 3)$  can be reached with different probabilities. We discuss some of the issues in Ref. [10]. We do not attempt a similar analysis here. However, we do calculate the same gap survival probability with DEDUCTOR changing only the ordering variable in order to see if one ordering gives a clearly better description of the Atlas data.

Given the theoretical issues, it is of interest to ask whether one gets anywhere near the Atlas data using DEDUCTOR with its LC+ treatment of color (which is nowhere near a full color treatment) and with the  $i\pi$  contributions from virtual graphs omitted in the current version of the program. Furthermore, it is of interest to investigate whether the choice of  $\Lambda$  ordering versus  $k_T$  ordering makes a difference and whether non-perturbative effects make a difference. We do not have code to match DEDUCTOR to an NLO perturbative calculation, so we cannot expect the accuracy of Ref. [101]. However, there is some advantage to this calculation because we can see how well DEDUCTOR by itself can do without matching its first emission to a perturbative result. We can then separately check how well a purely perturbative calculation does.

We begin with the question of whether, for a measurement controlled by a parameter  $p_T^{\text{cut}} = 20$  GeV, non-perturbative effects at a scale of 1 GeV might be important. To perturbative DEDUCTOR events we add an underlying event and then send the event to PYTHIA as described in Sec. II A. We calculate the difference

$$\Delta f = f(\text{DEDUCTOR \& PYTHIA}) - f(\text{DEDUCTOR}). \quad (22)$$

We display the results as a function of  $\bar{p}_T$  in Fig. 10 for the case  $2 < \Delta y < 3$ . There are some evident statistical fluctuations but the result is clear: there is an effect, but it is no larger than 5%. Since the non-perturbative effects make so little difference, in subsequent plots we work at just the

partonic level.

Now we examine the effects of logs of  $\bar{p}_T/p_T^{\text{cut}}$  and factors of  $\Delta y$  by using three different methods to calculate  $f$  as a function of  $\bar{p}_T$  in five different ranges of  $\Delta y$ . We show the results in Fig. 11 along with the data from Atlas [99].

We begin with the purely perturbative result (plotted as a green dash-dotted line) calculated at NLO according to Eq. (21). For very large  $\Delta y$  or  $\log(\bar{p}_T/p_T^{\text{cut}})$ , the perturbative result must fail because it does not sum large logarithmic factors. Indeed, we see that the perturbative result lies under the data for  $\alpha_s \Delta y \log(\bar{p}_T/p_T^{\text{cut}}) \gtrsim 1$ , for instance, for  $\bar{p}_T > 150$  GeV when  $4 < \Delta y < 5$ . However, it seems to us remarkable that the perturbative result is quite close to the data for smaller values of  $\bar{p}_T$  and  $\Delta y$  and that it is within 0.2 of the data for the whole range of  $\bar{p}_T$  and  $\Delta y$  for which data is available. This is the opposite qualitative conclusion to that obtained from a purely perturbative expansion [101] instead of Eq. (21). This suggests that while a summation of factors of  $\Delta y \log(\bar{p}_T/p_T^{\text{cut}})$  is very interesting for QCD theory, it is not numerically dominant in most of the range covered by the data.

We next turn to calculations with DEDUCTOR with two choices for the ordering variable, as described in Sec. II B. The results with the default ordering variable  $\Lambda$  are plotted in red while the results with  $k_T$  ordering are plotted in blue. We use the scale choices specified in Sec. II C. We see that the data are reasonably well described by DEDUCTOR with either  $\Lambda$  or  $k_T$  ordering. The match is closer with  $\Lambda$  ordering, but given the inherent uncertainties of a calculation with a leading order parton shower based on a leading order hard scattering, we judge that there is not a clear preference of one ordering choice over the other.

Ref. [101] found that a SHERPA leading order shower matched to  $\alpha_s^2 + \alpha_s^3$  perturbation theory for the hard scattering matched data very well. Since since the DEDUCTOR shower with either ordering variable starting from just an  $\alpha_s^2$  hard scattering is not to far from the higher order perturbative results, we expect that the DEDUCTOR showers matched to NLO perturbative results would also agree well with data.

#### IV. CONCLUSIONS

We have modified DEDUCTOR to include

- the ability to change between the default virtuality based ordering parameter  $\Lambda$  and a transverse momentum ordering parameter  $k_T$ ;

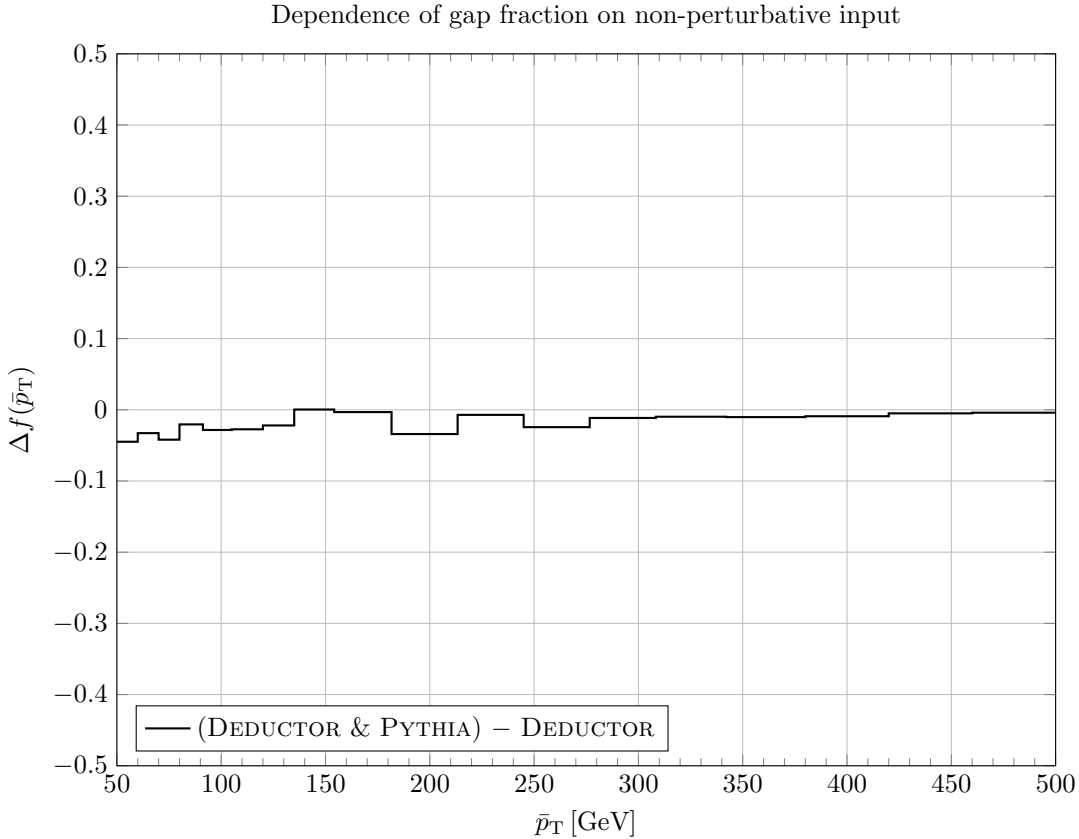


FIG. 10. Change  $\Delta f$  in the gap fraction for  $2 < \Delta y < 3$  when nonperturbative effects are added.

- the ability to include non-perturbative physics by adding a simple underlying event and sending events to PYTHIA for hadronization;
- a summation of threshold logarithms according to the lowest order version of the formulation in Ref. [4].

A version of the threshold factors was given in Ref. [13], but in this version, there was an unphysical dependence on low momentum physics. With this earlier formulation one had to use an *ad hoc* cutoff parameter to get physically reasonable results. The all-order formulation of Ref. [4] shows how the threshold factor should appear.

In this paper, we have used the new version of DEDUCTOR to investigate two features of jet physics. We are using a lowest order parton shower. A leading order shower can be matched to an NLO perturbative calculation. In principle, this is straightforward [63–83]. For DEDUCTOR, we would use the construction of Ref. [4], in which the subtraction terms that remove the divergences from the NLO calculation are directly related to the shower splitting functions. However, we have

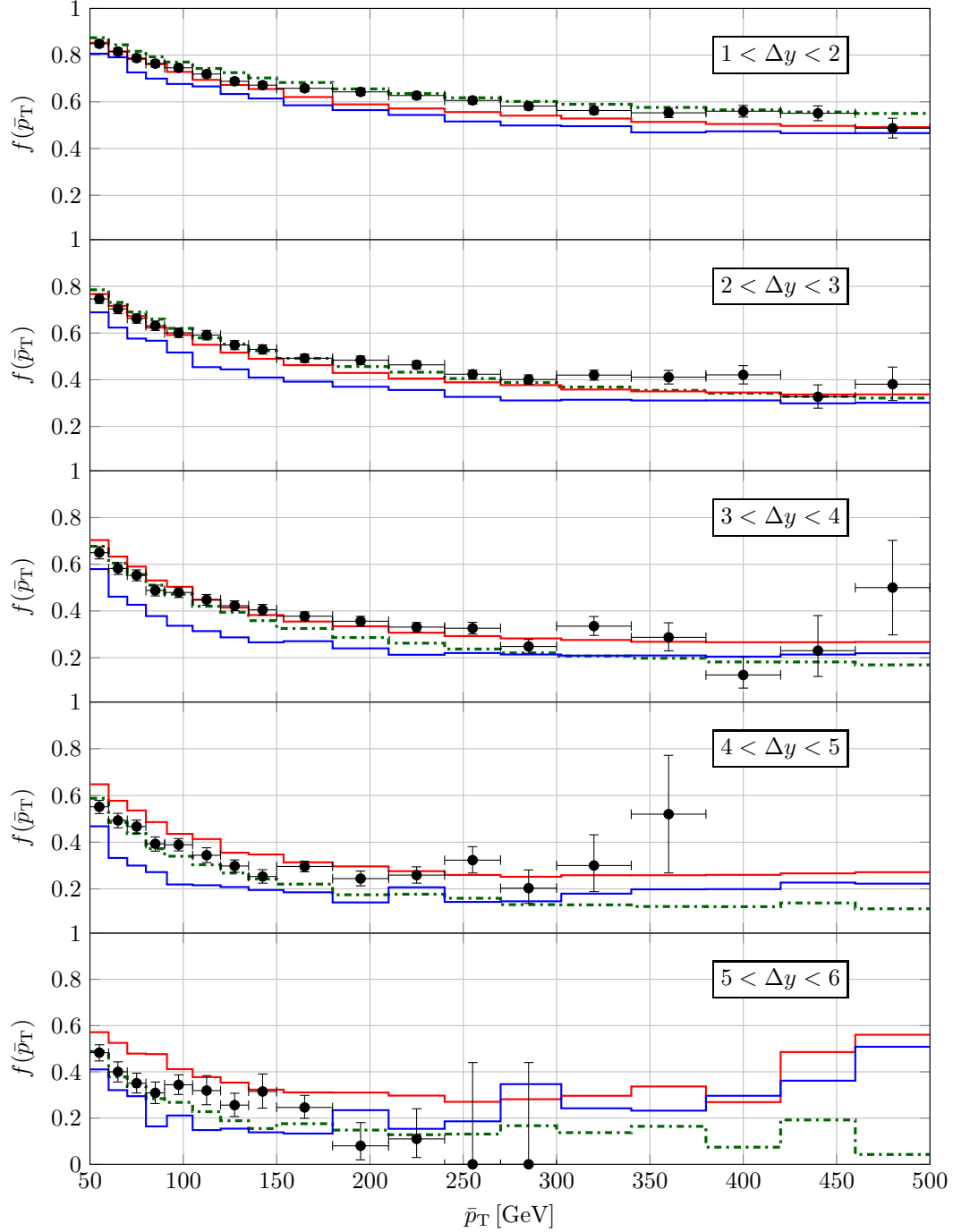


FIG. 11. Gap fraction for various  $y$  values. The black points with error bars are Atlas data [99]. The green dash-dotted histogram is NLO perturbation theory [102] as defined by Eq. (21). The red (higher) solid histogram is DEDUCTOR with  $\Lambda$  ordering, while the blue (lower) solid histogram is DEDUCTOR with  $k_T$  ordering.

not carried out this construction. Matching would improve the precision of the results and would remove much of the sensitivity to the starting conditions of the shower. Without matching, we can look for large effects, but we miss the finer details. Nevertheless, we find that there are interesting large effects.

We first investigated the one jet inclusive cross section at large values of the jet transverse momentum  $P_T$ . We find that non-perturbative physics is not important for this cross section. We find that the difference between a jet and a parton is numerically highly significant: the jet cross section is substantially affected by parton showering. The cross section after showering is smaller than it was before showering, particularly for smaller values of the jet radius  $R$ . This effect depends on what is built into the parton shower. We see a more pronounced effect with DEDUCTOR than with DIRE or PYTHIA. It appears that DEDUCTOR has more wide angle emissions that are away from the strict soft emission limit. We also find that the threshold factor is important at large  $P_T$ . In fact, with DEDUCTOR, the threshold factor is large enough to cancel the loss of jet cross section from showering, leaving a cross section that is close to the NLO jet cross section. Other parton shower programs lack the threshold summation. We also find that with  $k_T$  ordering, the threshold factor is smaller than with  $\Lambda$  ordering, but is still substantial.

We next investigated the gap fraction: in events with two two high- $P_T$  jets that are separated by a large difference  $\Delta y$  in rapidity, this is the fraction of events in which there are no jets above a minimum  $p_T$  in the rapidity interval between the jets. There are a number of subtle theoretical issues associated with the gap fraction, so it is not obvious how well a parton shower should describe the physics. We find that non-perturbative physics is not important for the gap fraction. We then find that DEDUCTOR with  $\Lambda$  ordering reproduces reasonably well Atlas data for the gap fraction. With  $k_T$  ordering, the agreement is also reasonably good. Finally, an NLO perturbative calculation without showering matches the experimental results well when  $\bar{p}_T/p_T^{\min}$  and  $\Delta y$  are not too large and is not far off in the entire range of  $\bar{p}_T/p_T^{\min}$  and  $\Delta y$  for which there are data.

## ACKNOWLEDGMENTS

This work was supported in part by the United States Department of Energy under grant DE-SC0011640. Some of the project was carried out while the authors were at the Munich Institute for Astro- and Particle Physics program “Automated, resummed and effective: precision computations for the LHC and beyond.” We thank the MIAPP for providing a stimulating research environment. We thank Mrinal Dasgupta and Gavin Salam for helpful conversations about the relation between

parton evolution and jets. We thank Werner Vogelsang for providing us with the de Florian, Hinderer, Mukherjee, Ringer, Vogelsang code for threshold corrections to the jet cross section.

### Appendix A: The threshold factor

The threshold factor, as given in Eq. (9) is

$$\mathcal{U}_{\mathcal{V}}(\mu_f^2, \mu_H^2) = \mathbb{T} \exp\left(\int_{\mu_f^2}^{\mu_H^2} \frac{d\mu^2}{\mu^2} \mathcal{S}_{\mathcal{V}}(\mu^2)\right). \quad (\text{A1})$$

This is in the notation of Ref. [4]. It is instructive to see how Eq. (A1) is translated to the notation of Ref. [13]. The first step is to approximate Eq. (A1) by using only the first order version,  $\mathcal{S}_{\mathcal{V}}^{(1)}(\mu^2)$ , of  $\mathcal{S}_{\mathcal{V}}(\mu^2)$ . According to Eq. (D.26) of Ref. [4], we have

$$\mathcal{S}_{\mathcal{V}}^{(1)}(\mu^2) = \left[ \mu_s^2 \frac{\partial}{\partial \mu_s^2} \mathcal{V}_{\text{ao}}^{(1)}(\mu^2, \mu_s^2) \right]_{\mu_s^2 = \mu^2} - \mathcal{F}^{-1}(\mu^2) \left[ \mu^2 \frac{d\mathcal{F}(\mu^2)}{d\mu^2} \right]. \quad (\text{A2})$$

Here  $\mathcal{V}_{\text{ao}}^{(1)}(\mu^2, \mu_s^2)$  is the first order version of the operator called  $\mathcal{V}$  in Ref. [4]. Since there is a different operator defined in Ref. [13] with the name  $\mathcal{V}$ , we add a subscript “ao” to indicate that it is the operator called  $\mathcal{V}$  in the *all order* notation. This operator has two scale arguments:  $\mu^2$  is the factorization and renormalization scale while  $\mu_s^2$  is the shower scale, to be discussed below. After differentiating with respect to  $\mu_s^2$ , we set  $\mu_s^2 = \mu^2$ . The operator  $\mathcal{F}(\mu^2)$  multiplies by the right product of parton distribution functions and a parton luminosity factor to make a cross section [4, 13]. The parton distribution functions depend on  $\mu^2$ . Differentiating with respect to  $\mu^2$  gives the evolution kernel for the parton distribution functions convolved with the parton distribution functions. Here, working to lowest order, we would use the order  $\alpha_s$  evolution kernel.

The operator  $\mathcal{V}_{\text{ao}}^{(1)}(\mu^2, \mu_s^2)$  has three parts,

$$\mathcal{V}_{\text{ao}}^{(1)}(\mu^2, \mu_s^2) = \mathcal{V}_{\text{ao}}^{(1,0)}(\mu^2, \mu_s^2) + \mathcal{V}_{\text{ao}}^{(0,1)}(\mu^2, \mu_s^2) + \mathcal{V}_{\text{ao}}^{\text{pdf}}(\mu^2). \quad (\text{A3})$$

Here  $\mathcal{V}_{\text{ao}}^{\text{pdf}}(\mu^2)$  is related to the definition of the parton distribution functions. It does not depend on  $\mu_s^2$ , so it does not contribute once we differentiate with respect to  $\mu_s^2$ . The operator  $\mathcal{V}_{\text{ao}}^{(1,0)}$  comes from real emission graphs and  $\mathcal{V}_{\text{ao}}^{(0,1)}$  comes from virtual graphs. These operators leave the number of partons, their momenta, and their flavors unchanged. They are defined by specifying what  $(1|\mathcal{V}_{\text{ao}}^{(1)}$  is, where multiplying by  $(1|$  indicates making a completely inclusive measurement, in which we sum over flavors, integrate over momenta, and take the trace over spins and colors. The definition (at first order) is

$$\begin{aligned} (1|\mathcal{V}_{\text{ao}}^{(1,0)}(\mu^2, \mu_s^2) &= (1|\mathcal{F}(\mu^2)\mathcal{D}^{(1,0)}(\mu^2, \mu_s^2)\mathcal{F}^{-1}(\mu^2), \\ (1|\mathcal{V}_{\text{ao}}^{(0,1)}(\mu^2, \mu_s^2) &= (1|\mathcal{D}^{(0,1)}(\mu^2, \mu_s^2). \end{aligned} \quad (\text{A4})$$

The operator  $\mathcal{D}^{(1,0)}(\mu^2, \mu_s^2)$  represents real emission Feynman graphs in which we integrate over the scale of the emission up to an upper limit  $\mu_s^2$ . For a  $\Lambda$  ordered shower, the emission scale is  $\Lambda^2$  as defined in Eq. (1). Then the integrals in  $\mathcal{D}^{(1,0)}(\mu^2, \mu_s^2)$  contain a factor  $\Theta(\Lambda^2 - \mu_s^2)$ . Differentiating with respect to  $\mu_s^2$  as in Eq. (A2) then gives a factor  $\delta(\Lambda^2 - \mu_s^2)$ . Similarly  $\mathcal{D}^{(0,1)}(\mu^2, \mu_s^2)$  represents virtual Feynman graphs in which we integrate over a scale variable  $\Lambda^2$  [13] with a factor  $\Theta(\Lambda^2 < \mu_s^2)$ . Again, differentiation gives a factor  $\delta(\Lambda^2 - \mu_s^2)$ .

In the notation of Ref. [13], the names are different:

$$\begin{aligned} \left[ \mu_s^2 \frac{\partial}{\partial \mu_s^2} \mathcal{V}_{\text{ao}}^{(1,0)}(\mu^2, \mu_s^2) \right]_{\mu_s^2 = \mu^2} &\rightarrow \mathcal{V}(\mu^2), \\ \left[ \mu_s^2 \frac{\partial}{\partial \mu_s^2} \mathcal{V}_{\text{ao}}^{(0,1)}(\mu^2, \mu_s^2) \right]_{\mu_s^2 = \mu^2} &\rightarrow -\{\mathcal{S}(\mu^2) - \mathcal{S}_{i\pi}(\mu^2)\} + \mathcal{F}^{-1}(\mu^2) \left[ \mu^2 \frac{d\mathcal{F}(\mu^2)}{d\mu^2} \right]. \end{aligned} \quad (\text{A5})$$

There are two things to note. First, as defined in Ref. [13],  $\mathcal{S}(\mu^2)$  includes both the contribution from virtual graphs, called  $\mathcal{S}^{\text{pert}}(\mu^2)$ , and the contribution from the evolution of the parton distribution functions that we remove in Eq. (A5). See Eq. (A8) below. Second, some of the virtual graphs have an imaginary part. Then  $\mathcal{S}(\mu^2)$  includes a contribution  $\mathcal{S}_{i\pi}(\mu^2)$  from the imaginary parts. However,  $\mathcal{S}_{i\pi}(\mu^2)$  does not contribute to  $\mathcal{V}_{\text{ao}}^{(0,1)}$  because  $(1|\mathcal{S}_{i\pi}(\mu^2) = 0$ . We include only the real part of the one loop graphs in the exponent of the threshold factor.

We are thus able to represent the threshold factor  $\mathcal{U}_{\mathcal{V}}$  from Eq. (9) in the notation of ref. [13] and our earlier papers. We use  $\Lambda^2$  defined in Eq. (1) as the hardness scale  $\mu^2$  and use the shower time

$$t = \log(Q_0^2/\Lambda^2) \quad (\text{A6})$$

as the integration variable instead of  $\mu^2$ . This gives the representation

$$\mathcal{U}_{\mathcal{V}}(t_{\text{f}}^2, t_{\text{H}}^2) = \mathbb{T} \exp \left( \int_{t_{\text{f}}^2}^{t_{\text{H}}^2} dt [\mathcal{V}(t) - \{\mathcal{S}(t) - \mathcal{S}_{i\pi}(t)\}] \right) \quad (\text{A7})$$

Here the operator  $\mathcal{S}(\mu^2)$  has two contributions:

$$\mathcal{S}(t) = \mathcal{S}^{\text{pert}}(t) - \mathcal{F}(t)^{-1} \left[ \frac{d}{dt} \mathcal{F}(t) \right]. \quad (\text{A8})$$

The operator  $\mathcal{S}^{\text{pert}}(t)$  is calculated from one loop virtual Feynman graphs. We remove the contribution  $\mathcal{S}_{i\pi}(\mu^2)$  from the imaginary part of the one loop graphs.

We could simply use  $\mathcal{S}(t)$  and  $\mathcal{V}(t)$  as given in Ref. [13] to construct the threshold factor (11). However, we have found that some of the integrations that go into these operators can be performed so that they are accurate in a wider range of the kinematic variables compared to Ref. [13]. Thus we use the improved versions of  $\mathcal{S}(t)$  and  $\mathcal{V}(t)$  in DEDUCTOR v. 2.1.0. We explain the changes relative to Ref. [13] in the subsections that follow.

## 1. Initial state virtual contribution

In this subsection, we examine the contribution to  $\mathcal{S}$  from a virtual graph in which a gluon is emitted from the initial state line and absorbed by a final state line. We modify the calculation in Appendix C.3 of Ref. [13] to make it accurate in a wider range, as explained below.

### a. The momenta

The exchanged gluon carries momentum  $q$  from line “a,” which carries momentum  $p_a$  into the graph, to line  $k$ , which carries momentum  $p_k$  out of the graph, so that, inside the loop, line “a” carries momentum  $p_a - q$  and line  $k$  carries momentum  $p_k - q$ .

We denote the components of  $q$  and  $p_k$  in the rest frame of  $Q$

$$\begin{aligned} q &= (1 - z') p_a + \xi p_b + q_\perp , \\ p_k &= (1 - z_k) p_a + \xi_k p_b + p_{k,\perp} , \end{aligned} \tag{A9}$$

where  $0 < z_k < 1$  and

$$\xi_k = \frac{\mathbf{p}_{k,\perp}^2}{(1 - z_k)Q^2} . \tag{A10}$$

Here we need  $(1 - z_k) > 0$  so that  $p_k$  has positive + momentum (momentum along  $p_a$ ). Also, we need  $(1 - z_k) < 1$  because no final state particle can have more + momentum than is contained in  $p_a$ . Then also

$$\begin{aligned} p_a - q &= z' p_a - \xi p_b - q_\perp , \\ p_k - q &= (z' - z_k) p_a + (\xi_k - \xi) p_b + p_{k,\perp} - q_\perp . \end{aligned} \tag{A11}$$

### b. The integral

We start with integral representing the exchange in Coulomb gauge,

$$\begin{aligned} &\int dt [S_{ak}^L(\{p, f\}_m; t) + S_{ka}^L(\{p, f\}_m; t)] \\ &= i \frac{\alpha_s}{(2\pi)^3} \int d^4q \frac{2J_a(p_a, q) \cdot D(q) \cdot J_k(p_k, q)}{(-(q - p_a)^2 - i\epsilon)(-(q - p_k)^2 - i\epsilon)(q^2 + i\epsilon)} . \end{aligned} \tag{A12}$$

Here, following the notation in Ref. [13], the superscript L refers to a virtual graph to the left of the final state cut. In Ref. [13] we used the eikonal approximation, in which  $J_a(p_a, q) \rightarrow 2p_a$ ,  $J_k(p_k, q) \rightarrow 2p_k$ ,  $-(q - p_a)^2 \rightarrow 2q \cdot p_a$ , and  $-(q - p_k)^2 \rightarrow 2q \cdot p_k$ . This is a good approximation if  $q$  is small, but  $q$  is perhaps not always small, and if we make this approximation we may even allow

$q$  to become much larger than it becomes in the exact integral. For this reason, we do not make the eikonal approximation to start with here.

For  $S_{ak}^L$  use the dimensionless integration variable  $y = -(q - p_a)^2/Q^2$ , which is used to define the shower time for the virtual splitting through  $t = -\log[y Q^2/(2p_a \cdot Q_0)]$ , where  $Q_0$  is the total momentum of the final state at the start of the shower. As in Ref. [13], we use the approximation  $y \ll 1$ . The calculation in Ref. [13] also used the approximation  $y \ll 1 - \cos \theta_{ak}$ . However, it is certainly possible to have a final state parton  $k$  that is very nearly collinear with the momentum  $p_a$  of the incoming beam parton. For this reason, in this appendix we seek to modify the calculation in Ref. [13] so that it is valid also when  $1 - \cos \theta_{ak} \lesssim y$ . We thus suppose that  $p_k$  is nearly collinear with  $p_a$  and concentrate on the integration region in which  $q$  is nearly collinear with  $p_a$ . In Ref. [13], we first performed the integration over  $q^0$  by contour integration, then separated  $S_{ak}^L$  and  $S_{ka}^L$ . In  $S_{ak}^L$ , we inserted a factor  $\delta(y + (q - p_a)^2/Q^2)$  to eliminate one dimension of the integration over  $\vec{q}$ , then performed the rest of the integration over  $\vec{q}$  analytically in the small  $y$  limit. We will see that a very simple change is needed in the integral that represents  $S_{ak}^L(\{p, f\}_m; t)$  in [13]. To motivate this change, the most straightforward path would be to expand the denominators in eq. (A12) in powers of the angles of  $\vec{q}$  and  $\vec{p}_k$  with respect to  $\vec{p}_a$ , then perform the  $q^0$  integration and proceed along the lines of Ref. [13]. However, we find it more instructive to introduce null-plane coordinates for the momenta, as we have done in Eqs. (A9) and (A11). Then in the collinear limits, the component of  $q$  along  $p_a$  is large while the component along  $p_b$  is small. We then start by performing the integral over the small component of  $q$  by contour integration.

*c. Performing the  $\xi$  integration*

We are particularly interested in the denominators in Eq. (A12):

$$\begin{aligned} \frac{1}{q^2 + i\epsilon} &= \frac{1}{(1 - z')\xi Q^2 - \mathbf{q}_\perp^2 + i\epsilon} , \\ \frac{1}{-(q - p_a)^2 - i\epsilon} &= \frac{1}{z'\xi Q^2 + \mathbf{q}_\perp^2 - i\epsilon} , \\ \frac{1}{-(q - p_k)^2 - i\epsilon} &= \frac{1}{(z' - z_k)(\xi - \xi_k)Q^2 + (\mathbf{p}_{k,\perp} - \mathbf{q}_\perp)^2 - i\epsilon} . \end{aligned} \tag{A13}$$

We will integrate over  $z'$ . We examine the integration region in which the components along  $p_a$  of  $q$ ,  $p_a - q$ , and  $p_k - q$  are all positive. That is, we integrate over the region  $z_k < z' < 1$ . Other regions for  $z'$  give qualitatively different results. We first integrate over  $\xi$ , noting that in the region  $z_k < z' < 1$ , the first denominator factor has a pole in the lower half  $\xi$  plane, while the other two

poles are in the upper half  $\xi$  plane. We close the  $\xi$  contour in the lower half plane so that we pick up the pole at  $\xi = \xi_q$  where

$$\xi_q = \frac{\mathbf{q}_\perp^2}{(1-z')Q^2} \quad (\text{A14})$$

This gives

$$\begin{aligned} & \int dt [S_{ak}^L(\{p, f\}_m; t) + S_{ka}^L(\{p, f\}_m; t)] \\ &= \frac{\alpha_s}{(2\pi)^2} \int_{z_k}^1 \frac{dz'}{1-z'} \int d\mathbf{q}_\perp \frac{J_a(p_a, q) \cdot D(q) \cdot J_k(p_k, q)}{D_a D_k} . \end{aligned} \quad (\text{A15})$$

Here

$$\begin{aligned} D_a &= z' \xi_q Q^2 + \mathbf{q}_\perp^2 , \\ D_k &= (z' - z_k)(\xi_q - \xi_k) Q^2 + (\mathbf{p}_{k,\perp} - \mathbf{q}_\perp)^2 . \end{aligned} \quad (\text{A16})$$

*d. Structure of the result*

The two denominators are

$$\begin{aligned} D_a &= \frac{1}{1-z'} \mathbf{q}_\perp^2 , \\ D_k &= \frac{z' - z_k}{1-z'} \mathbf{q}_\perp^2 - \frac{z' - z_k}{1-z_k} \mathbf{p}_{k,\perp}^2 + (\mathbf{p}_{k,\perp} - \mathbf{q}_\perp)^2 . \end{aligned} \quad (\text{A17})$$

We define the virtuality variable  $y$  by

$$yQ^2 = D_a . \quad (\text{A18})$$

Then there is a relation between  $\mathbf{q}_\perp^2$ ,  $y$ , and  $z$

$$\mathbf{q}_\perp^2 = (1-z')yQ^2 . \quad (\text{A19})$$

We could have tried this using the eikonal approximation. Then

$$\begin{aligned} -(q - p_a)^2 &= 2q \cdot p_a - q^2 \rightarrow 2q \cdot p_a , \\ -(q - p_k)^2 &= 2q \cdot p_k - q^2 \rightarrow 2q \cdot p_k . \end{aligned} \quad (\text{A20})$$

We then evaluate this by setting  $\xi$  to  $\xi_q$ . But with  $\xi \rightarrow \xi_q$ ,  $q^2 \rightarrow 0$ . Thus we get exactly the same result for  $D_a$  and  $D_k$ . However, if we make the replacements eq. (A20) before performing the  $\xi$  integration, the locations of poles can shift between the upper and lower half  $\xi$  planes, so that the results change.

The result for  $D_k$  emerges in the form

$$D_k = \frac{1 - z'}{1 - z_k} \mathbf{p}_{k,\perp}^2 + \frac{1 - z_k}{1 - z'} \mathbf{q}^2 - 2\mathbf{q}_\perp \cdot \mathbf{p}_{k,\perp} . \quad (\text{A21})$$

This is the same as the result that we had, simply expanded differently. In this form, it is evident that  $D_k$  is linear in  $q$  and  $p_k$ . That is,  $D_k$  is proportional to  $\lambda$  under the scaling  $(1 - z_k) \rightarrow \lambda(1 - z_k)$ ,  $\mathbf{p}_{k,\perp} \rightarrow \lambda\mathbf{p}_{k,\perp}$ . It is also proportional to  $\lambda$  under the scaling  $(1 - z) \rightarrow \lambda(1 - z)$ ,  $\mathbf{q}_\perp \rightarrow \lambda\mathbf{q}_\perp$ .

It is perhaps also worthwhile to note that

$$D_k = (1 - z_k)(1 - z') \left( \frac{\mathbf{p}_{k,\perp}}{1 - z_k} - \frac{\mathbf{q}_\perp}{1 - z'} \right)^2 . \quad (\text{A22})$$

With this form, we see that  $D_k$  is invariant under a null-plane boost:  $\mathbf{p}_{k,\perp} \rightarrow \mathbf{p}_{k,\perp} + (1 - z_k)\mathbf{v}$ ,  $\mathbf{q}_\perp \rightarrow \mathbf{q}_\perp + (1 - z')\mathbf{v}$ . It is also invariant under a  $z$  boost:  $(1 - z_k) \rightarrow \lambda(1 - z_k)$ ,  $(1 - z') \rightarrow \lambda(1 - z')$ .

*e. Results for the integral*

We can now make use of our results in Ref. [13]. Our integral is in Appendix C.3. There, we used the eikonal approximation, where we should have used the full energy denominators. However, we have seen that using the full energy denominators gives the same result as using the eikonal approximation except that using the full energy denominators tells us where to put bounds on the integration over the component of  $q$  along  $p_a$ .

From Eq. (C.63) of Ref. [13], we have

$$S_{\text{ab}}^{\text{L}}(\{p, f\}_m; t) \approx \frac{\alpha_s}{2\pi} [-1 + i\pi] . \quad (\text{A23})$$

Also, (noting that  $2|\vec{p}_a| = E_Q$  in the result from Eq. (C.91) of Ref. [13]), we have

$$S_{\text{aa}}^{\text{L}}(\{p, f\}_m; t) = -\frac{\alpha_s}{2\pi} \left( \frac{\gamma_{f_a}}{2C_{f_a}} + \log(y) + 1 \right) . \quad (\text{A24})$$

In Appendix C.3 of Ref. [13], there are two parts of the result for  $S_{\text{ak}}^{\text{L}}$ ,

$$S_{\text{ak}}^{\text{L}}(\{p, f\}_m; t) = S_{\text{ak}}^{\text{L}}(\{p, f\}_m; t; \text{dipole}) + S_{\text{aa}}^{\text{L}}(\{p, f\}_m; t; \text{eikonal}) \quad (\text{A25})$$

The first part is

$$\begin{aligned} S_{\text{ak}}^{\text{L}}(\{p, f\}_m; t; \text{dipole}) &\approx -\frac{\alpha_s}{2\pi} \int_{1-M/|\vec{p}_a|}^{1-y} \frac{dz}{\sqrt{(1-z)^2 + y^2/\psi_{\text{ak}}^2}} \\ &= -\frac{\alpha_s}{2\pi} \log \left( \frac{M/|\vec{p}_a| + \sqrt{M^2/|\vec{p}_a|^2 + y^2/\psi_{\text{ak}}^2}}{y \left( 1 + \sqrt{1 + 1/\psi_{\text{ak}}^2} \right)} \right) . \end{aligned} \quad (\text{A26})$$

where, according to Eq. (A.13) of Ref. [13],

$$\psi_{ak} = \frac{1 - \cos \theta_{ak}}{\sqrt{8(1 + \cos \theta_{ak})}}. \quad (\text{A27})$$

This definition gives

$$1 + \sqrt{1 + 1/\psi_{ak}^2} = \frac{4}{1 - \cos \theta_{ak}}. \quad (\text{A28})$$

The variable  $z$  in eq. (A26) is almost the same as the variable  $z'$  of this appendix:  $z = z' - y$ . The  $z$  integration has a lower bound  $1 - M/|\vec{p}_a|$ . In Ref. [13], we took  $M$  to be a large positive number. However, we now recognize that, at least when  $1 - \cos \theta_{ak} \ll 1$ , the lower bound on the  $z$  integration should be  $z_k + y$ , which we can approximate by just  $z_k$ . Thus we should set  $M/|\vec{p}_a| = 1 - z_k$ . This gives

$$S_{ak}^L(\{p, f\}_m; t; \text{dipole}) = -\frac{\alpha_s}{2\pi} \log \left( \frac{1 - z_k + \sqrt{(1 - z_k)^2 + y^2/\psi_{ak}^2}}{4y/(1 - \cos \theta_{ak})} \right). \quad (\text{A29})$$

For  $S_{ll}^L(\{p, f\}_m; t; \text{eikonal})$ , we have from Eq. (C.58) of Ref. [13]

$$\begin{aligned} S_{aa}^L(\{p, f\}_m; t; \text{eikonal}) &= \frac{\alpha_s}{2\pi} \int_{1-M/|\vec{p}_a|}^{1-y} dz \frac{(1-z) - y}{(1-z)^2} \\ &= \frac{\alpha_s}{2\pi} \left[ \log \left( \frac{M/|\vec{p}_a|}{y} \right) - 1 + \frac{y}{M/|\vec{p}_a|} \right]. \end{aligned} \quad (\text{A30})$$

We set  $M/|\vec{p}_a| = 1 - z_k$  to obtain

$$S_{aa}^L(\{p, f\}_m; t; \text{eikonal}) = \frac{\alpha_s}{2\pi} \left[ \log \left( \frac{1 - z_k}{y} \right) - 1 + \frac{y}{1 - z_k} \right]. \quad (\text{A31})$$

When we add  $S_{ak}^L(\{p, f\}_m; t; \text{dipole})$  and  $S_{aa}^L(\{p, f\}_m; t; \text{eikonal})$  according to Eq. (A25), we obtain

$$S_{ak}^L(\{p, f\}_m; t) = -\frac{\alpha_s}{2\pi} \left\{ \log \left( \frac{1 - z_k + \sqrt{(1 - z_k)^2 + y^2/\psi_{ak}^2}}{4(1 - z_k)/(1 - \cos \theta_{ak})} \right) + 1 - \frac{y}{1 - z_k} \right\}. \quad (\text{A32})$$

We treat  $z_k$  as some finite number, not close to 1. We suppose that  $y \ll 1$  but we do not assume that  $y$  is small compared to  $\psi_{ak}$ . Then we can neglect  $y/(1 - z_k)$ . Also, we can simplify the argument of the logarithm. Then we get

$$S_{ak}^L(\{p, f\}_m; t) = -\frac{\alpha_s}{2\pi} \left\{ \log \left( \frac{1 + \sqrt{1 + y^2/[\psi_{ak}^2(1 - z_k)^2]}}{4/(1 - \cos \theta_{ak})} \right) + 1 \right\}. \quad (\text{A33})$$

When  $y \ll 1 - \cos \theta_{ak}$  we recover the result of Ref. [13], but now we have a result that works also for  $1 - \cos \theta_{ak} \gtrsim y$ .

For later use, we write the log term as an integral :

$$\log \left( \frac{1 + \sqrt{1 + y^2 / [\psi_{ak}^2 (1 - z_k)^2]}}{4 / (1 - \cos \theta_{ak})} \right) \approx \int_{z_k}^{1/(1+y)} dz \left[ \frac{1}{\sqrt{(1-z)^2 + y^2 / \psi_{ak}^2}} - \frac{1}{1-z} \right]. \quad (\text{A34})$$

(Here we have replaced  $1 - y$  by  $1/(1 + y)$  for  $y \ll 1$  in the upper limit of the integral.)

*f. Assembling the result*

We now write the total contribution to  $\mathcal{S}$  from virtual emissions from the initial state parton “a” as (See eqs. (C.3) and (C.4) of Ref. [13])

$$\begin{aligned} & \mathcal{S}_a^{\text{pert}}(t) | \{p, f, c', c\}_m \rangle \\ &= \left\{ \sum_{k \neq a, b} S_{ak}^L ([(\mathbf{T}_a \cdot \mathbf{T}_k) \otimes 1] + [1 \otimes (\mathbf{T}_a \cdot \mathbf{T}_k)]) \right. \\ & \quad + \text{Re } S_{ab}^L ([(\mathbf{T}_a \cdot \mathbf{T}_b) \otimes 1] + [1 \otimes (\mathbf{T}_a \cdot \mathbf{T}_b)]) \\ & \quad + \text{Im } S_{ab}^L ([(\mathbf{T}_a \cdot \mathbf{T}_b) \otimes 1] - [1 \otimes (\mathbf{T}_a \cdot \mathbf{T}_b)]) \\ & \quad \left. + S_{aa}^L ([(\mathbf{T}_a \cdot \mathbf{T}_a) \otimes 1] + [1 \otimes (\mathbf{T}_a \cdot \mathbf{T}_b)]) \right\} \\ & \quad \times | \{p, f, c', c\}_m \rangle. \end{aligned} \quad (\text{A35})$$

We use Eq. (A33) for  $S_{ak}^L$  and Eq. (A24) for  $S_{aa}^L$  and Eq. (A23) for  $S_{ab}^L$ . Then

$$\begin{aligned} & \mathcal{S}_a^{\text{pert}}(t) | \{p, f, c', c\}_m \rangle \\ &= \frac{\alpha_s}{2\pi} \left\{ \sum_{k \neq a, b} \left[ -\log \left( \frac{1 + \sqrt{1 + y^2 / [\psi_{ak}^2 (1 - z_k)^2]}}{4 / (1 - \cos \theta_{ak})} \right) - 1 \right] \right. \\ & \quad \times ([(\mathbf{T}_a \cdot \mathbf{T}_k) \otimes 1] + [1 \otimes (\mathbf{T}_a \cdot \mathbf{T}_k)]) \\ & \quad - ([(\mathbf{T}_a \cdot \mathbf{T}_b) \otimes 1] + [1 \otimes (\mathbf{T}_a \cdot \mathbf{T}_b)]) \\ & \quad + i\pi ([(\mathbf{T}_a \cdot \mathbf{T}_b) \otimes 1] - [1 \otimes (\mathbf{T}_a \cdot \mathbf{T}_b)]) \\ & \quad \left. - \left[ \frac{\gamma_a}{2C_a} + \log(y) + 1 \right] ([(\mathbf{T}_a \cdot \mathbf{T}_a) \otimes 1] + [1 \otimes (\mathbf{T}_a \cdot \mathbf{T}_b)]) \right\} \\ & \quad \times | \{p, f, c', c\}_m \rangle. \end{aligned} \quad (\text{A36})$$

The terms  $-1$  times color operators cancel because  $\sum_k (\mathbf{T}_a \cdot \mathbf{T}_k) = 0$ . Also  $(\mathbf{T}_a \cdot \mathbf{T}_a) = C_a 1$ . Also, for  $k = b$  we have  $1/\psi_{ab} = 0$ , so

$$\log \left( \frac{1 + \sqrt{1 + y^2 / [\psi_{ab}^2 (1 - z_k)^2]}}{4 / (1 - \cos \theta_{ab})} \right) = 0. \quad (\text{A37})$$

This means that the sum over  $k$  in the first term can include  $k = b$ . Thus

$$\begin{aligned}
& \mathcal{S}_a^{\text{pert}}(t) | \{p, f, c', c\}_m \rangle \\
&= \frac{\alpha_s}{2\pi} \left\{ - \sum_{k \neq a} \log \left( \frac{1 + \sqrt{1 + y^2 / [\psi_{ak}^2 (1 - z_k)^2]}}{4 / (1 - \cos \theta_{ak})} \right) \right. \\
&\quad \times ([(\mathbf{T}_a \cdot \mathbf{T}_k) \otimes 1] + [1 \otimes (\mathbf{T}_a \cdot \mathbf{T}_k)]) \\
&\quad + i\pi ([(\mathbf{T}_a \cdot \mathbf{T}_b) \otimes 1] - [1 \otimes (\mathbf{T}_a \cdot \mathbf{T}_b)]) \\
&\quad \left. - 2C_a \left[ \frac{\gamma_a}{2C_a} + \log(y) \right] [1 \otimes 1] \right\} \\
&\quad \times | \{p, f, c', c\}_m \rangle .
\end{aligned} \tag{A38}$$

To this we have to add the contribution from parton evolution, using eqs. (6.6), (6.7), and (6.9) of Ref. [13]. This gives us

$$\begin{aligned}
& \mathcal{S}_a(t) | \{p, f, c', c\}_m \rangle \\
&= \frac{\alpha_s}{2\pi} \left\{ - \sum_{k \neq a} \log \left( \frac{1 + \sqrt{1 + y^2 / [\psi_{ak}^2 (1 - z_k)^2]}}{4 / (1 - \cos \theta_{ak})} \right) \right. \\
&\quad \times ([(\mathbf{T}_a \cdot \mathbf{T}_k) \otimes 1] + [1 \otimes (\mathbf{T}_a \cdot \mathbf{T}_k)]) \\
&\quad + i\pi ([(\mathbf{T}_a \cdot \mathbf{T}_b) \otimes 1] - [1 \otimes (\mathbf{T}_a \cdot \mathbf{T}_b)]) \\
&\quad - 2C_a \left[ \frac{\gamma_a}{2C_a} + \log(y) \right] [1 \otimes 1] \\
&\quad \left. + \sum_{\hat{a}} \int_0^1 dz \left( \frac{1}{z} P_{a\hat{a}}(z) \frac{f_{\hat{a}/A}(\eta_a/z, yQ^2)}{f_{a/A}(\eta_a, yQ^2)} - \delta_{a\hat{a}} \left[ \frac{2C_a}{1-z} - \gamma_a \right] \right) [1 \otimes 1] \right\} \\
&\quad \times | \{p, f, c', c\}_m \rangle .
\end{aligned} \tag{A39}$$

The terms proportional to  $\gamma_a$  cancel. Also, we can use

$$2C_a [1 \otimes 1] = ([(\mathbf{T}_a \cdot \mathbf{T}_a) \otimes 1] + [1 \otimes (\mathbf{T}_a \cdot \mathbf{T}_a)]) = - \sum_{k \neq a} ([(\mathbf{T}_a \cdot \mathbf{T}_k) \otimes 1] + [1 \otimes (\mathbf{T}_a \cdot \mathbf{T}_k)]) \tag{A40}$$

to associate the  $\log(y)$  term with the first line. This gives us

$$\begin{aligned}
& \mathcal{S}_a(t) | \{p, f, c', c\}_m \rangle \\
&= \frac{\alpha_s}{2\pi} \left\{ - \sum_{k \neq a, b} \log \left( \frac{1 + \sqrt{1 + y^2 / [\psi_{ak}^2 (1 - z_k)^2]}}{4y / (1 - \cos \theta_{ak})} \right) \right. \\
&\quad \times ([(\mathbf{T}_a \cdot \mathbf{T}_k) \otimes 1] + [1 \otimes (\mathbf{T}_a \cdot \mathbf{T}_k)]) \\
&\quad + i\pi ([(\mathbf{T}_a \cdot \mathbf{T}_b) \otimes 1] - [1 \otimes (\mathbf{T}_a \cdot \mathbf{T}_b)]) \\
&\quad \left. + \sum_{\hat{a}} \int_0^1 \frac{dz}{z} \left( P_{a\hat{a}}(z) \frac{f_{\hat{a}/A}(\eta_a/z, yQ^2)}{f_{a/A}(\eta_a, yQ^2)} - \delta_{a\hat{a}} \frac{2zC_a}{1-z} \right) [1 \otimes 1] \right\} \\
&\quad \times | \{p, f, c', c\}_m \rangle .
\end{aligned} \tag{A41}$$

## 2. Initial state real contribution

We need  $\mathcal{V}_a(t)$ . From Eq. (B.63) of Ref. [13], we have the probability for emitting a parton from initial state gluon ‘‘a’’ at shower time  $t$ , assuming  $y \ll 1$ ,

$$\begin{aligned}
& \mathcal{V}_a(t) | \{p, f, c', c\}_m \rangle \\
&= \frac{\alpha_s}{2\pi} \int_0^{1/(1+y)} \frac{dz}{z} \sum_{\hat{a}} \frac{f_{\hat{a}/A}(\eta_a/z, yQ^2)}{f_{a/A}(\eta_a, yQ^2)} \\
&\quad \times \left\{ \frac{1}{2C_a} \left( P_{\hat{a}a}(z) - \delta_{\hat{a}a} \frac{2zC_a}{1-z} \right) ([(\mathbf{T}_a \cdot \mathbf{T}_a) \otimes 1] + [1 \otimes (\mathbf{T}_a \cdot \mathbf{T}_a)]) \right. \\
&\quad \left. - \delta_{\hat{a}a} \sum_{k \neq a} z v(y, z, \theta_{ak}) ([(\mathbf{T}_a \cdot \mathbf{T}_k) \otimes 1] + [1 \otimes (\mathbf{T}_a \cdot \mathbf{T}_k)]) \right\} \\
&\quad \times | \{p, f, c', c\}_m \rangle .
\end{aligned} \tag{A42}$$

Here

$$v(y, z, \theta_{ak}) = \int_0^{2\pi} \frac{d\phi}{2\pi} \frac{\hat{p}_k \cdot \hat{p}_a}{\hat{p}_{m+1} \cdot \hat{p}_k + yz \hat{p}_k \cdot \hat{Q}} . \tag{A43}$$

In Eq. (B.63) of Ref. [13], we used an approximate form for  $v(y, z, \xi_{ak})$ , but here, we calculate it exactly:

$$v(y, z, \theta_{ak}) = \frac{z}{1-z} \frac{1+y}{1+zy} \frac{1-\delta}{\sqrt{(1-\delta)^2 + 4x^2\delta}} + \frac{1}{1+zy} . \tag{A44}$$

Here

$$x = \frac{zy}{1-z} \tag{A45}$$

and

$$\delta = (1 + zy)(1 + y)(1 + \cos \theta_{ak})/2. \quad (\text{A46})$$

We note that  $x$  runs from 0 to 1 when  $z$  ranges from 0 to its upper limit,  $1/(1+y)$ , and that  $\delta > 0$ . However,  $\delta$  can be larger than 1 when  $\theta_{ak}$  is small.

We can simplify Eq. (A42) a little by using  $\mathbf{T}_a \cdot \mathbf{T}_a = C_a$ , giving us

$$\begin{aligned} & \mathcal{V}_a(t) | \{p, f, c', c\}_m \rangle \\ &= \frac{\alpha_s}{2\pi} \int_0^{1/(1+y)} \frac{dz}{z} \sum_{\hat{a}} \frac{f_{\hat{a}/A}(\eta_a/z, yQ^2)}{f_{a/A}(\eta_a, yQ^2)} \\ & \times \left\{ \left( P_{\hat{a}a}(z) - \delta_{\hat{a}a} \frac{2zC_a}{1-z} \right) [1 \otimes 1] \right. \\ & \quad \left. - \delta_{\hat{a}a} \sum_{k \neq a} z v(y, z, \theta_{ak}) \left( [(\mathbf{T}_a \cdot \mathbf{T}_k) \otimes 1] + [1 \otimes (\mathbf{T}_a \cdot \mathbf{T}_k)] \right) \right\} \\ & \times | \{p, f, c', c\}_m \rangle. \end{aligned} \quad (\text{A47})$$

### 3. The initial state cross section changing exponent

Now we need  $\mathcal{V}_a(t) - \mathcal{S}_a(t)$ . Using eqs. (A41) and (A47), we have

$$\begin{aligned} & [\mathcal{V}_a(t) - \mathcal{S}_a(t)] | \{p, f, c', c\}_m \rangle \\ &= \frac{\alpha_s}{2\pi} \left\{ \sum_{k \neq a, b} \log \left( \frac{1 + \sqrt{1 + y^2 / [\psi_{ak}^2 (1 - z_k)^2]}}{4y / (1 - \cos \theta_{ak})} \right) \right. \\ & \quad \times \left( [(\mathbf{T}_a \cdot \mathbf{T}_k) \otimes 1] + [1 \otimes (\mathbf{T}_a \cdot \mathbf{T}_k)] \right) \\ & \quad - i\pi \left( [(\mathbf{T}_a \cdot \mathbf{T}_b) \otimes 1] - [1 \otimes (\mathbf{T}_a \cdot \mathbf{T}_b)] \right) \\ & \quad - \sum_{\hat{a}} \int_0^1 \frac{dz}{z} \left( P_{\hat{a}a}(z) \frac{f_{\hat{a}/A}(\eta_a/z, yQ^2)}{f_{a/A}(\eta_a, yQ^2)} - \delta_{\hat{a}a} \frac{2zC_a}{1-z} \right) [1 \otimes 1] \\ & \quad + \sum_{\hat{a}} \int_0^{1/(1+y)} \frac{dz}{z} \frac{f_{\hat{a}/A}(\eta_a/z, yQ^2)}{f_{a/A}(\eta_a, yQ^2)} \left( P_{\hat{a}a}(z) - \delta_{\hat{a}a} \frac{2zC_a}{1-z} \right) [1 \otimes 1] \\ & \quad - \int_0^{1/(1+y)} \frac{dz}{z} \frac{f_{a/A}(\eta_a/z, yQ^2)}{f_{a/A}(\eta_a, yQ^2)} \sum_{k \neq a} z v(y, z, \theta_{ak}) \\ & \quad \left. \times \left( [(\mathbf{T}_a \cdot \mathbf{T}_k) \otimes 1] + [1 \otimes (\mathbf{T}_a \cdot \mathbf{T}_k)] \right) \right\} \\ & \times | \{p, f, c', c\}_m \rangle. \end{aligned} \quad (\text{A48})$$

We can simplify this. We replace

$$P_{\hat{a}a}(z) = P_{\hat{a}a}^{\text{reg}}(z) + \delta_{\hat{a}a} \frac{2zC_a}{1-z}. \quad (\text{A49})$$

This gives

$$\begin{aligned} & [\mathcal{V}_a(t) - \mathcal{S}_a(t)] | \{p, f, c', c\}_m) \\ &= \frac{\alpha_s}{2\pi} \left\{ \sum_{k \neq a, b} \log \left( \frac{1 + \sqrt{1 + y^2 / [\psi_{ak}^2 (1 - z_k)^2]}}{4y / (1 - \cos \theta_{ak})} \right) \right. \\ & \quad \times ([(\mathbf{T}_a \cdot \mathbf{T}_k) \otimes 1] + [1 \otimes (\mathbf{T}_a \cdot \mathbf{T}_k)]) \\ & \quad - i\pi ([(\mathbf{T}_a \cdot \mathbf{T}_b) \otimes 1] - [1 \otimes (\mathbf{T}_a \cdot \mathbf{T}_b)]) \\ & \quad - \sum_{\hat{a}} \int_0^1 \frac{dz}{z} P_{\hat{a}a}^{\text{reg}}(z) \frac{f_{\hat{a}/A}(\eta_a/z, yQ^2)}{f_{a/A}(\eta_a, yQ^2)} [1 \otimes 1] \\ & \quad + \int_0^1 \frac{dz}{z} \left( 1 - \frac{f_{a/A}(\eta_a/z, \mu_a^2(t))}{f_{a/A}(\eta_a, \mu_a^2(t))} \right) \frac{2zC_a}{1-z} [1 \otimes 1] \\ & \quad + \sum_{\hat{a}} \int_0^{1/(1+y)} \frac{dz}{z} \frac{f_{\hat{a}/A}(\eta_a/z, yQ^2)}{f_{a/A}(\eta_a, yQ^2)} P_{\hat{a}a}^{\text{reg}}(z) [1 \otimes 1] \\ & \quad - \int_0^{1/(1+y)} \frac{dz}{z} \frac{f_{a/A}(\eta_a/z, yQ^2)}{f_{a/A}(\eta_a, yQ^2)} \sum_{k \neq a} z v(y, z, \theta_{ak}) \\ & \quad \left. \times ([(\mathbf{T}_a \cdot \mathbf{T}_k) \otimes 1] + [1 \otimes (\mathbf{T}_a \cdot \mathbf{T}_k)]) \right\} \\ & \quad \times | \{p, f, c', c\}_m) . \end{aligned} \quad (\text{A50})$$

The two terms involving  $P_{\hat{a}a}^{\text{reg}}$  cancel except for not having the same limits of integration. We divide the last term into three terms by using

$$\begin{aligned} \frac{f_{a/A}(\eta_a/z, yQ^2)}{f_{a/A}(\eta_a, yQ^2)} v(y, z, \xi_k) &= - \left( 1 - \frac{f_{a/A}(\eta_a/z, yQ^2)}{f_{a/A}(\eta_a, yQ^2)} \right) \frac{1}{1-z} \\ & \quad + \left( 1 - \frac{f_{a/A}(\eta_a/z, yQ^2)}{f_{a/A}(\eta_a, yQ^2)} \right) \left( \frac{1}{1-z} - v(y, z, \theta_{ak}) \right) \\ & \quad + v(y, z, \theta_{ak}) . \end{aligned} \quad (\text{A51})$$

This gives

$$\begin{aligned}
& [\mathcal{V}_a(t) - \mathcal{S}_a(t)] | \{p, f, c', c\}_m \rangle \\
&= \frac{\alpha_s}{2\pi} \left\{ \sum_{k \neq a, b} \log \left( \frac{1 + \sqrt{1 + y^2 / [\psi_{ak}^2 (1 - z_k)^2]}}{4y / (1 - \cos \theta_{ak})} \right) \right. \\
&\quad \times ([(\mathbf{T}_a \cdot \mathbf{T}_k) \otimes 1] + [1 \otimes (\mathbf{T}_a \cdot \mathbf{T}_k)]) \\
&\quad - i\pi ([(\mathbf{T}_a \cdot \mathbf{T}_b) \otimes 1] - [1 \otimes (\mathbf{T}_a \cdot \mathbf{T}_b)]) \\
&\quad - \sum_{\hat{a}} \int_{1/(1+y)}^1 \frac{dz}{z} P_{a\hat{a}}^{\text{reg}}(z) \frac{f_{\hat{a}/A}(\eta_a/z, yQ^2)}{f_{a/A}(\eta_a, yQ^2)} [1 \otimes 1] \\
&\quad + \int_0^1 \frac{dz}{z} \left( 1 - \frac{f_{a/A}(\eta_a/z, yQ^2)}{f_{a/A}(\eta_a, yQ^2)} \right) \frac{2zC_a}{1-z} [1 \otimes 1] \\
&\quad + \int_0^{1/(1+y)} \frac{dz}{z} \left( 1 - \frac{f_{a/A}(\eta_a/z, yQ^2)}{f_{a/A}(\eta_a, yQ^2)} \right) \frac{z}{1-z} \\
&\quad \times \sum_{k \neq a} ([(\mathbf{T}_a \cdot \mathbf{T}_k) \otimes 1] + [1 \otimes (\mathbf{T}_a \cdot \mathbf{T}_k)]) \\
&\quad - \int_0^{1/(1+y)} \frac{dz}{z} \left( 1 - \frac{f_{a/A}(\eta_a/z, yQ^2)}{f_{a/A}(\eta_a, yQ^2)} \right) \sum_{k \neq a} \left( \frac{z}{1-z} - z v(y, z, \theta_{ak}) \right) \\
&\quad \times ([(\mathbf{T}_a \cdot \mathbf{T}_k) \otimes 1] + [1 \otimes (\mathbf{T}_a \cdot \mathbf{T}_k)]) \\
&\quad - \int_0^{1/(1+y)} \frac{dz}{z} \sum_{k \neq a} z v(y, z, \theta_{ak}) \\
&\quad \times ([(\mathbf{T}_a \cdot \mathbf{T}_k) \otimes 1] + [1 \otimes (\mathbf{T}_a \cdot \mathbf{T}_k)]) \left. \right\} \\
&\quad \times | \{p, f, c', c\}_m \rangle .
\end{aligned} \tag{A52}$$

In the first of the new terms, we can use

$$\sum_{k \neq a} ([(\mathbf{T}_a \cdot \mathbf{T}_k) \otimes 1] + [1 \otimes (\mathbf{T}_a \cdot \mathbf{T}_k)]) = -2C_a [1 \otimes 1] \tag{A53}$$

Then this term almost cancels the term that precedes it, leaving

$$\begin{aligned}
& [\mathcal{V}_a(t) - \mathcal{S}_a(t)] | \{p, f, c', c\}_m \rangle \\
&= \frac{\alpha_s}{2\pi} \left\{ \sum_{k \neq a, b} \log \left( \frac{1 + \sqrt{1 + y^2 / [\psi_{ak}^2 (1 - z_k)^2]}}{4y / (1 - \cos \theta_{ak})} \right) \right. \\
&\quad \times ([(\mathbf{T}_a \cdot \mathbf{T}_k) \otimes 1] + [1 \otimes (\mathbf{T}_a \cdot \mathbf{T}_k)]) \\
&\quad - i\pi ([(\mathbf{T}_a \cdot \mathbf{T}_b) \otimes 1] - [1 \otimes (\mathbf{T}_a \cdot \mathbf{T}_b)]) \\
&\quad - \sum_{\hat{a}} \int_{1/(1+y)}^1 \frac{dz}{z} P_{a\hat{a}}^{\text{reg}}(z) \frac{f_{\hat{a}/A}(\eta_a/z, yQ^2)}{f_{a/A}(\eta_a, yQ^2)} [1 \otimes 1] \\
&\quad + \int_{1/(1+y)}^1 \frac{dz}{z} \left( 1 - \frac{f_{a/A}(\eta_a/z, yQ^2)}{f_{a/A}(\eta_a, yQ^2)} \right) \frac{2zC_a}{1-z} [1 \otimes 1] \\
&\quad - \int_0^{1/(1+y)} \frac{dz}{z} \left( 1 - \frac{f_{a/A}(\eta_a/z, yQ^2)}{f_{a/A}(\eta_a, yQ^2)} \right) \sum_{k \neq a} \left( \frac{z}{1-z} - z v(y, z, \theta_{ak}) \right) \\
&\quad \times ([(\mathbf{T}_a \cdot \mathbf{T}_k) \otimes 1] + [1 \otimes (\mathbf{T}_a \cdot \mathbf{T}_k)]) \\
&\quad \left. - \int_0^{1/(1+y)} \frac{dz}{z} \sum_{k \neq a} z v(y, z, \theta_{ak}) ([(\mathbf{T}_a \cdot \mathbf{T}_k) \otimes 1] + [1 \otimes (\mathbf{T}_a \cdot \mathbf{T}_k)]) \right\} \\
&\quad \times | \{p, f, c', c\}_m \rangle .
\end{aligned} \tag{A54}$$

Finally, we combine the first and last terms, using the representation (A34) of the logarithm in the first term as an integral over  $z$ . We have not yet specified the scale argument of  $\alpha_s$ . We note that the virtuality of an initial state splitting is  $yQ^2$  and its transverse momentum (as defined in DEDUCTOR) is  $(1-z)yQ^2$ . We set the  $\alpha_s$  scale to either  $\lambda_R yQ^2$  or  $(1-z)\lambda_R yQ^2$ , where we use  $\lambda_R = \exp(-[C_A(67 - 3\pi^2) - 10 n_f]/[3(33 - 2 n_f)]) \approx 0.4$  [104]. (In  $\lambda_R$ , the number  $n_f$  of active flavors depends on the scale.) We also insert an infrared cutoff  $(1-z)yQ^2 > m_\perp^2(a)$  where  $m_\perp(a)$  is the quark mass when  $a$  is a bottom or charm flavor and is otherwise of order 1 GeV. The result

is not sensitive to the infrared cutoff. This gives

$$\begin{aligned}
& [\mathcal{V}_a(t) - \mathcal{S}_a(t)] | \{p, f, c', c\}_m \rangle \\
&= \left\{ \int_{1/(1+y)}^1 \frac{dz}{z} \frac{\alpha_s((1-z)\lambda_R y Q^2)}{2\pi} \theta((1-z)yQ^2 > m_\perp^2(a)) \right. \\
&\quad \times \left( 1 - \frac{f_{a/A}(\eta_a/z, yQ^2)}{f_{a/A}(\eta_a, yQ^2)} \right) \frac{2zC_a}{1-z} [1 \otimes 1] \\
&\quad - \sum_{\hat{a}} \int_{1/(1+y)}^1 \frac{dz}{z} \frac{\alpha_s(\lambda_R y Q^2)}{2\pi} \theta((1-z)yQ^2 > m_\perp^2(a)) \\
&\quad \times P_{a\hat{a}}^{\text{reg}}(z) \frac{f_{\hat{a}/A}(\eta_a/z, yQ^2)}{f_{a/A}(\eta_a, yQ^2)} [1 \otimes 1] \\
&\quad - \int_0^{1/(1+y)} \frac{dz}{z} \frac{\alpha_s((1-z)\lambda_R y Q^2)}{2\pi} \theta((1-z)yQ^2 > m_\perp^2(a)) \\
&\quad \times \left( 1 - \frac{f_{a/A}(\eta_a/z, yQ^2)}{f_{a/A}(\eta_a, yQ^2)} \right) \sum_{k \neq a} \left( \frac{z}{1-z} - z v(y, z, \theta_{ak}) \right) \\
&\quad \times ([(\mathbf{T}_a \cdot \mathbf{T}_k) \otimes 1] + [1 \otimes (\mathbf{T}_a \cdot \mathbf{T}_k)]) \\
&\quad + \sum_{k \neq a, b} I_k(y, \xi_k, z_k) ([(\mathbf{T}_a \cdot \mathbf{T}_k) \otimes 1] + [1 \otimes (\mathbf{T}_a \cdot \mathbf{T}_k)]) \\
&\quad \left. - i\pi \frac{\alpha_s(\lambda_R y Q^2)}{2\pi} ([(\mathbf{T}_a \cdot \mathbf{T}_b) \otimes 1] - [1 \otimes (\mathbf{T}_a \cdot \mathbf{T}_b)]) \right\} \\
&\quad \times | \{p, f, c', c\}_m \rangle,
\end{aligned} \tag{A55}$$

where we have defined

$$\begin{aligned}
I_k(y, \xi_k, z_k) &= \int_0^{1/(1+y)} dz \frac{\alpha_s((1-z)\lambda_R y Q^2)}{2\pi} \theta((1-z)yQ^2 > m_\perp^2(a)) \\
&\quad \times \left[ \frac{\theta(z > z_k)}{\sqrt{(1-z)^2 + y^2/\psi_{ak}^2}} - \frac{\theta(z > z_k)}{1-z} - v(y, z, \theta_{ak}) \right].
\end{aligned} \tag{A56}$$

Eq. (A55) replaces Eq. (7.21) of Ref. [13]. The first term is the main threshold term. The second is a correction from  $P_{a\hat{a}}^{\text{reg}}$ . The third term is corrected from what we had because we use the function  $v(y, z, \xi_k)$  instead of our previous approximation to it. The fourth term was approximated by zero in Ref. [13]. The fifth term is from the  $i\pi$  part of the virtual corrections. This is probability preserving and, according to Eq. (A7), is not included in the threshold correction.

- 
- [1] M. Bahr *et al.*, *Herwig++ Physics and Manual*, *Eur. Phys. J. C* **58**, 639 (2008) [INSPIRE].  
[2] T. Sjostrand *et al.*, *An Introduction to PYTHIA 8.2*, *Comput. Phys. Commun.* **191**, 159 (2015) [INSPIRE].

- [3] T. Gleisberg, S. Hoeche, F. Krauss, M. Schonherr, S. Schumann, F. Siegert and J. Winter, *Event generation with SHERPA 1.1*, **JHEP 0902, 007 (2009)** [[INSPIRE](#)].
- [4] Z. Nagy and D. E. Soper, *What is a parton shower?*, arXiv:1705.08093 [hep-ph] [[INSPIRE](#)].
- [5] Z. Nagy and D. E. Soper, *Parton showers with quantum interference*, **JHEP 0709, 114 (2007)** [[INSPIRE](#)].
- [6] Z. Nagy and D. E. Soper, *Parton showers with quantum interference: Leading color, spin averaged*, **JHEP 0803, 030 (2008)** [[INSPIRE](#)].
- [7] Z. Nagy and D. E. Soper, *Parton showers with quantum interference: Leading color, with spin*, **JHEP 0807, 025 (2008)** [[INSPIRE](#)].
- [8] Z. Nagy and D. E. Soper, *Parton shower evolution with subleading color*, **JHEP 1206, 044 (2012)** [[INSPIRE](#)].
- [9] Z. Nagy and D. E. Soper, *A parton shower based on factorization of the quantum density matrix*, **JHEP 1406, 097 (2014)** [[INSPIRE](#)].
- [10] Z. Nagy and D. E. Soper, *Ordering variable for parton showers*, **JHEP 1406, 178 (2014)** [[INSPIRE](#)].
- [11] Z. Nagy and D. E. Soper, *Parton distribution functions in the context of parton showers*, **JHEP 1406, 179 (2014)** [[INSPIRE](#)].
- [12] Z. Nagy and D. E. Soper, *Effects of subleading color in a parton shower*, **JHEP 1507, 119 (2015)** [[INSPIRE](#)].
- [13] Z. Nagy and D. E. Soper, *Summing threshold logs in a parton shower*, **JHEP 1610, 019 (2016)** [[INSPIRE](#)].
- [14] G. F. Sterman, *Summation of Large Corrections to Short Distance Hadronic Cross-Sections*, **Nucl. Phys. B 281, 310 (1987)** [[INSPIRE](#)].
- [15] D. Appell, G. F. Sterman and P. B. Mackenzie, *Soft Gluons and the Normalization of the Drell-Yan Cross-section*, **Nucl. Phys. B 309, 259 (1988)** [[INSPIRE](#)].
- [16] S. Catani and L. Trentadue, *Resummation of the QCD Perturbative Series for Hard Processes*, **Nucl. Phys. B 327, 323 (1989)** [[INSPIRE](#)].
- [17] S. Catani, B. R. Webber and G. Marchesini, *QCD coherent branching and semiinclusive processes at large  $x$* , **Nucl. Phys. B 349, 635 (1991)** [[INSPIRE](#)].
- [18] L. Magnea, *All Order Summation and Two Loop Results for the Drell-Yan Cross-section*, **Nucl. Phys. B 349, 703 (1991)** [[INSPIRE](#)].
- [19] G. P. Korchemsky and G. Marchesini, *Resummation of large infrared corrections using Wilson loops*, **Phys. Lett. B 313, 433 (1993)** [[INSPIRE](#)].
- [20] S. Catani, M. L. Mangano, P. Nason and L. Trentadue, *The Resummation of soft gluons in hadronic collisions*, **Nucl. Phys. B 478, 273 (1996)** [[INSPIRE](#)].
- [21] H. Contopanagos, E. Laenen and G. F. Sterman, *Sudakov factorization and resummation*, **Nucl. Phys. B 484, 303 (1997)** [[INSPIRE](#)].
- [22] N. Kidonakis and G. F. Sterman, *Resummation for QCD hard scattering*,

- Nucl. Phys. B **505**, 321 (1997) [INSPIRE].
- [23] N. Kidonakis, G. Oderda and G. F. Sterman, *Threshold resummation for dijet cross-sections*, Nucl. Phys. B **525**, 299 (1998) [INSPIRE].
- [24] N. Kidonakis, G. Oderda and G. F. Sterman, *Evolution of color exchange in QCD hard scattering*, Nucl. Phys. B **531**, 365 (1998) [INSPIRE].
- [25] E. Laenen, G. Oderda and G. F. Sterman, *Resummation of threshold corrections for single particle inclusive cross-sections*, Phys. Lett. B **438**, 173 (1998) [INSPIRE].
- [26] S. Catani, M. L. Mangano and P. Nason, *Sudakov resummation for prompt photon production in hadron collisions*, JHEP **9807**, 024 (1998) [INSPIRE].
- [27] H. n. Li, *Unification of the  $k(T)$  and threshold resummations*, Phys. Lett. B **454**, 328 (1999) [INSPIRE].
- [28] N. Kidonakis and J. F. Owens, *Soft gluon resummation and NNLO corrections for direct photon production*, Phys. Rev. D **61**, 094004 (2000) [INSPIRE].
- [29] G. F. Sterman and W. Vogelsang, *Threshold resummation and rapidity dependence*, JHEP **0102**, 016 (2001) [INSPIRE].
- [30] N. Kidonakis and J. F. Owens, *Effects of higher order threshold corrections in high  $E(T)$  jet production*, Phys. Rev. D **63**, 054019 (2001) [INSPIRE].
- [31] E. Laenen, G. F. Sterman and W. Vogelsang, *Recoil and threshold corrections in short distance cross-sections*, Phys. Rev. D **63**, 114018 (2001) [INSPIRE].
- [32] A. Kulesza, G. F. Sterman and W. Vogelsang, *Joint resummation in electroweak boson production*, Phys. Rev. D **66**, 014011 (2002) [INSPIRE].
- [33] N. Kidonakis, *Next-to-next-to-next-to-leading-order soft-gluon corrections in hard-scattering processes near threshold*, Phys. Rev. D **73**, 034001 (2006) [INSPIRE].
- [34] A. Mukherjee and W. Vogelsang, *Threshold resummation for  $W$ -boson production at RHIC*, Phys. Rev. D **73**, 074005 (2006) [INSPIRE].
- [35] P. Bolzoni, *Threshold resummation of Drell-Yan rapidity distributions*, Phys. Lett. B **643**, 325 (2006) [INSPIRE].
- [36] D. de Florian and W. Vogelsang, *Resummed cross-section for jet production at hadron colliders*, Phys. Rev. D **76**, 074031 (2007) [INSPIRE].
- [37] V. Ravindran, J. Smith and W. L. van Neerven, *QCD threshold corrections to di-lepton and Higgs rapidity distributions beyond  $N^2LO$* , Nucl. Phys. B **767**, 100 (2007) [INSPIRE].
- [38] V. Ravindran and J. Smith, *Threshold corrections to rapidity distributions of  $Z$  and  $W^\pm$  bosons beyond  $N^2LO$  at hadron colliders*, Phys. Rev. D **76**, 114004 (2007) [INSPIRE].
- [39] M. Bonvini, S. Forte and G. Ridolfi, *Soft gluon resummation of Drell-Yan rapidity distributions: Theory and phenomenology*, Nucl. Phys. B **847**, 93 (2011) [INSPIRE].
- [40] M. Bonvini, S. Forte and G. Ridolfi, *The Threshold region for Higgs production in gluon fusion*, Phys. Rev. Lett. **109**, 102002 (2012) [INSPIRE].

- [41] D. de Florian, P. Hinderer, A. Mukherjee, F. Ringer and W. Vogelsang, *Approximate next-to-next-to-leading order corrections to hadronic jet production*, *Phys. Rev. Lett.* **112**, 082001 (2014) [INSPIRE].
- [42] S. Catani, L. Cieri, D. de Florian, G. Ferrera and M. Grazzini, *Threshold resummation at  $N^3LL$  accuracy and soft-virtual cross sections at  $N^3LO$* , *Nucl. Phys. B* **888**, 75 (2014) [INSPIRE].
- [43] T. Ahmed, M. K. Mandal, N. Rana and V. Ravindran, *Rapidity Distributions in Drell-Yan and Higgs Productions at Threshold to Third Order in QCD*, *Phys. Rev. Lett.* **113**, 212003 (2014) [INSPIRE].
- [44] M. Bonvini and S. Marzani, *Resummed Higgs cross section at  $N^3LL$* , *JHEP* **1409**, 007 (2014) [INSPIRE].
- [45] M. Bonvini *et al.*, *Parton distributions with threshold resummation*, *JHEP* **1509**, 191 (2015) [INSPIRE].
- [46] A. V. Manohar, *Deep inelastic scattering as  $x \rightarrow 1$  using soft collinear effective theory*, *Phys. Rev. D* **68**, 114019 (2003) [INSPIRE].
- [47] A. Idilbi and X. d. Ji, *Threshold resummation for Drell-Yan process in soft-collinear effective theory*, *Phys. Rev. D* **72**, 054016 (2005) [INSPIRE].
- [48] T. Becher and M. Neubert, *Threshold resummation in momentum space from effective field theory*, *Phys. Rev. Lett.* **97**, 082001 (2006) [INSPIRE].
- [49] T. Becher, M. Neubert and B. D. Pecjak, *Factorization and Momentum-Space Resummation in Deep-Inelastic Scattering*, *JHEP* **0701**, 076 (2007) [INSPIRE].
- [50] T. Becher, M. Neubert and G. Xu, *Dynamical Threshold Enhancement and Resummation in Drell-Yan Production*, *JHEP* **0807**, 030 (2008) [INSPIRE].
- [51] T. Becher and M. D. Schwartz, *Direct photon production with effective field theory*, *JHEP* **1002**, 040 (2010) [INSPIRE].
- [52] I. W. Stewart, F. J. Tackmann and W. J. Waalewijn, *Factorization at the LHC: From PDFs to Initial State Jets*, *Phys. Rev. D* **81**, 094035 (2010) [INSPIRE].
- [53] M. Beneke, P. Falgari and C. Schwinn, *Threshold resummation for pair production of coloured heavy ( $s$ )particles at hadron colliders*, *Nucl. Phys. B* **842**, 414 (2011) [INSPIRE].
- [54] C. W. Bauer, F. J. Tackmann, J. R. Walsh and S. Zuberi, *Factorization and Resummation for Dijet Invariant Mass Spectra*, *Phys. Rev. D* **85**, 074006 (2012) [INSPIRE].
- [55] Y. Wang, C. S. Li, Z. L. Liu and D. Y. Shao, *Threshold resummation for  $W^\pm Z$  and  $ZZ$  pair production at the LHC*, *Phys. Rev. D* **90**, 034008 (2014) [INSPIRE].
- [56] G. Lusterians, W. J. Waalewijn and L. Zeune, *Joint transverse momentum and threshold resummation beyond NLL*, *Phys. Lett. B* **762**, 447 (2016) [INSPIRE].
- [57] M. Bonvini, S. Forte, M. Ghezzi and G. Ridolfi, *Threshold Resummation in SCET vs. Perturbative QCD: An Analytic Comparison*, *Nucl. Phys. B* **861**, 337 (2012) [INSPIRE].
- [58] G. Sterman and M. Zeng, *Quantifying Comparisons of Threshold Resummations*, *JHEP* **1405**, 132 (2014) [INSPIRE].
- [59] M. Bonvini, S. Forte, G. Ridolfi and L. Rottoli, *Resummation prescriptions and ambiguities in SCET*

- vs. direct QCD: Higgs production as a case study*, **JHEP 1501**, 046 (2015) [INSPIRE].
- [60] S. Dulat *et al.*, *New parton distribution functions from a global analysis of quantum chromodynamics*, **Phys. Rev. D 93**, 033006 (2016) [INSPIRE].
- [61] M. Cacciari, G. P. Salam and G. Soyez, *The Anti- $k(t)$  jet clustering algorithm*, **JHEP 0804**, 063 (2008) [INSPIRE].
- [62] M. Cacciari, G. P. Salam and G. Soyez, *FastJet User Manual*, **Eur. Phys. J. C 72**, 1896 (2012) [INSPIRE].
- [63] S. Frixione and B. R. Webber, *Matching NLO QCD computations and parton shower simulations*, **JHEP 0206**, 029 (2002) [INSPIRE].
- [64] P. Nason, *A New method for combining NLO QCD with shower Monte Carlo algorithms*, **JHEP 0411**, 040 (2004) [INSPIRE].
- [65] S. Frixione, P. Nason and C. Oleari, *Matching NLO QCD computations with Parton Shower simulations: the POWHEG method*, **JHEP 0711**, 070 (2007) [INSPIRE].
- [66] K. Hamilton and P. Nason, *Improving NLO-parton shower matched simulations with higher order matrix elements*, **JHEP 1006**, 039 (2010) [INSPIRE].
- [67] S. Alioli, P. Nason, C. Oleari and E. Re, *A general framework for implementing NLO calculations in shower Monte Carlo programs: the POWHEG BOX*, **JHEP 1006**, 043 (2010) [INSPIRE].
- [68] R. Frederix and S. Frixione, *Merging meets matching in MC@NLO*, **JHEP 1212**, 061 (2012) [INSPIRE].
- [69] K. Hamilton, P. Nason and G. Zanderighi, *MINLO: Multi-Scale Improved NLO*, **JHEP 1210**, 155 (2012) [INSPIRE].
- [70] K. Hamilton, P. Nason, C. Oleari and G. Zanderighi, *Merging  $H/W/Z + 0$  and 1 jet at NLO with no merging scale: a path to parton shower + NNLO matching*, **JHEP 1305**, 082 (2013) [INSPIRE].
- [71] S. Höche, F. Krauss, M. Schonherr and F. Siegert, *QCD matrix elements + parton showers: The NLO case*, **JHEP 1304**, 027 (2013) [INSPIRE].
- [72] L. Lönnblad and S. Prestel, *Merging Multi-leg NLO Matrix Elements with Parton Showers*, **JHEP 1303**, 166 (2013) [INSPIRE].
- [73] S. Plätzer, *Controlling inclusive cross sections in parton shower + matrix element merging*, **JHEP 1308**, 114 (2013) [INSPIRE].
- [74] K. Hamilton, P. Nason, E. Re and G. Zanderighi, *NNLOPS simulation of Higgs boson production*, **JHEP 1310**, 222 (2013) [INSPIRE].
- [75] J. Alwall *et al.*, *The automated computation of tree-level and next-to-leading order differential cross sections, and their matching to parton shower simulations*, **JHEP 1407**, 079 (2014) [INSPIRE].
- [76] S. Alioli, C. W. Bauer, C. Berggren, F. J. Tackmann, J. R. Walsh and S. Zuberi, *Matching Fully Differential NNLO Calculations and Parton Showers*, **JHEP 1406**, 089 (2014) [INSPIRE].
- [77] M. Czakon, H. B. Hartanto, M. Kraus and M. Worek, *Matching the Nagy-Soper parton shower at next-to-leading order*, **JHEP 1506**, 033 (2015) [INSPIRE].

- [78] S. Jadach, W. Płaczek, S. Sapeta, A. Siódmok and M. Skrzypek, *Matching NLO QCD with parton shower in Monte Carlo scheme – the KrkNLO method*, **JHEP** **1510**, 052 (2015) [INSPIRE].
- [79] R. Frederix and K. Hamilton, *Extending the MINLO method*, **JHEP** **1605**, 042 (2016) [INSPIRE].
- [80] S. Höche, Y. Li and S. Prestel, *Higgs-boson production through gluon fusion at NNLO QCD with parton showers*, **Phys. Rev. D** **90**, 054011 (2014) [INSPIRE].
- [81] S. Höche, Y. Li and S. Prestel, *Drell-Yan lepton pair production at NNLO QCD with parton showers*, **Phys. Rev. D** **91**, 074015 (2015) [INSPIRE].
- [82] A. Buckley *et al.*, *General-purpose event generators for LHC physics*, **Phys. Rept.** **504**, 145 (2011) [INSPIRE].
- [83] T. Sjöstrand, *Status and developments of event generators*, **PoS LHCP** **2016**, 007 (2016) [arXiv:1608.06425 [hep-ph]] [INSPIRE].
- [84] S. D. Ellis, Z. Kunszt and D. E. Soper, *The One Jet Inclusive Cross-section at Order  $\alpha_s^3$ : Quarks and Gluons*, **Phys. Rev. Lett.** **64**, 2121 (1990) [INSPIRE].
- [85] M. Dasgupta, F. Dreyer, G. P. Salam and G. Soyez, *Small-radius jets to all orders in QCD*, **JHEP** **1504**, 039 (2015) [INSPIRE].
- [86] M. Dasgupta, F. A. Dreyer, G. P. Salam and G. Soyez, *Inclusive jet spectrum for small-radius jets*, **JHEP** **1606**, 057 (2016) [INSPIRE].
- [87] Z. B. Kang, F. Ringer and I. Vitev, *The semi-inclusive jet function in SCET and small radius resummation for inclusive jet production*, **JHEP** **1610**, 125 (2016) [INSPIRE].
- [88] J. Forshaw, J. Keates and S. Marzani, *Jet vetoing at the LHC*, **JHEP** **0907**, 023 (2009) [INSPIRE].
- [89] N. Kidonakis, G. Oderda and G. F. Sterman, *Evolution of color exchange in QCD hard scattering*, **Nucl. Phys. B** **531**, 365 (1998) [INSPIRE].
- [90] G. Oderda and G. F. Sterman, *Energy and color flow in dijet rapidity gaps*, **Phys. Rev. Lett.** **81**, 3591 (1998) [INSPIRE].
- [91] J. R. Forshaw, A. Kyrieleis and M. H. Seymour, *Gaps between jets in the high energy limit*, **JHEP** **0506**, 034 (2005) [INSPIRE].
- [92] M. Dasgupta and G. P. Salam, *Resummation of nonglobal QCD observables*, **Phys. Lett. B** **512**, 323 (2001) [INSPIRE].
- [93] C. F. Berger, T. Kucs and G. F. Sterman, *Energy flow in interjet radiation*, **Phys. Rev. D** **65**, 094031 (2002) [INSPIRE].
- [94] M. Dasgupta and G. P. Salam, *Accounting for coherence in interjet  $E(t)$  flow: A Case study*, **JHEP** **0203**, 017 (2002) [INSPIRE].
- [95] R. B. Appleby and M. H. Seymour, *Nonglobal logarithms in interjet energy flow with  $kt$  clustering requirement*, **JHEP** **0212**, 063 (2002) [INSPIRE].
- [96] J. R. Forshaw, A. Kyrieleis and M. H. Seymour, *Super-leading logarithms in non-global observables in QCD?*, **JHEP** **0608**, 059 (2006) [INSPIRE].
- [97] J. R. Forshaw, A. Kyrieleis and M. H. Seymour, *Super-leading logarithms in non-global observables in*

- QCD: Colour basis independent calculation*, [JHEP 0809, 128 \(2008\)](#) [[INSPIRE](#)].
- [98] R. M. Duran Delgado, J. R. Forshaw, S. Marzani and M. H. Seymour, *The dijet cross section with a jet veto* [JHEP 1108, 157 \(2011\)](#) [[INSPIRE](#)].
- [99] G. Aad *et al.* [ATLAS Collaboration], *Measurement of dijet production with a veto on additional central jet activity in pp collisions at  $\sqrt{s} = 7$  TeV using the ATLAS detector*, [JHEP 1109, 053 \(2011\)](#) [[INSPIRE](#)].
- [100] S. Alioli, J. R. Andersen, C. Oleari, E. Re and J. M. Smillie, *Probing higher-order corrections in dijet production at the LHC*, [Phys. Rev. D 85, 114034 \(2012\)](#) [[INSPIRE](#)].
- [101] S. Hoeche and M. Schonherr, *Uncertainties in next-to-leading order plus parton shower matched simulations of inclusive jet and dijet production*, [Phys. Rev. D 86, 094042 \(2012\)](#) [[INSPIRE](#)].
- [102] Z. Nagy, *Next-to-leading order calculation of three jet observables in hadron hadron collision*, [Phys. Rev. D 68, 094002 \(2003\)](#) [[INSPIRE](#)].
- [103] Y. Hatta, C. Marquet, C. Royon, G. Soyez, T. Ueda and D. Werder, *A QCD description of the ATLAS jet veto measurement*, [Phys. Rev. D 87, 054016 \(2013\)](#) [[INSPIRE](#)].
- [104] R. K. Ellis, G. Marchesini and B. R. Webber, *Soft Radiation in Parton Parton Scattering*, [Nucl. Phys. B 286, 643 \(1987\)](#) Erratum: [[Nucl. Phys. B 294, 1180 \(1987\)](#)] [[INSPIRE](#)].